Inner membrane complex proteomics reveals a palmitoylation cascade regulating intraerythrocytic development of malaria parasite

Pengge Qian [1, 4], Xu Wang[1, 4], Chuan-Qi Zhong[1, 4], Jiaxu Wang[2, 4], Mengya Cai[1], Wang Nguitragool[3], Jian Li [1,*], Huiting Cui [1,*], Jing Yuan[1,*]

[1] State Key Laboratory of Cellular Stress Biology, Innovation Center for Cell Signal Network, School of Life Sciences, Xiamen University, Xiamen, Fujian 361102, China

[2] Xiamen Center for Disease Control and Prevention, Xiamen, Fujian 361021, China

[3] Department of Molecular Tropical Medicine and Genetics, Faculty of Tropical Medicine, Mahidol University, Ratchathewi, 10400, Bangkok, Thailand.

[4] These authors contributed equally

*Correspondence email: yuanjing@xmu.edu.cn, huitingcui@xmu.edu.cn, or jianli_204@xmu.edu.cn

Abstract

Malaria is caused by infection of the erythrocytes by the parasites *Plasmodium*. Inside the erythrocytes, the parasites multiply via schizogony, an unconventional cell division mode. The Inner Membrane Complex (IMC), an organelle located beneath the parasite plasma membrane, serving as the platform for protein anchorage, is essential for schizogony. So far, complete repertoire of IMC proteins and their localization determinants remain unclear. Here we used biotin ligase (TurboID)-based proximity labelling to compile the proteome of the schizont IMC of rodent malaria parasite *Plasmodium yoelii.* In total, 300 TurboID-interacting proteins were identified. 19 of the 22 selected candidates were confirmed to localize in the IMC, indicating good reliability. In light of the existing palmitome of *Plasmodium falciparum*, 83 proteins of the *P. yoelii* IMC proteome are potentially palmitoylated. We further identified DHHC2 as the major resident palmitoyl-acyl-transferase of the IMC. Depletion of DHHC2 led to defective schizont segmentation and growth arrest both *in vitro* and *in vivo*. DHHC2 was found to palmitoylate two critical IMC proteins CDPK1 and GAP45 for their IMC localization.

In summary, this study reports an inventory of new IMC proteins and demonstrates a central role of DHHC2 in governing IMC localization of proteins during the schizont development.

Introduction

Malaria, a human scourge caused by the protozoans of the genus *Plasmodium*, affects more than 200 million people and is responsible for approximately half a million deaths in 2019 [1]. The symptoms of malaria are caused by the intraerythrocytic proliferation of the parasites. After erythrocyte invasion, the parasites replicate via schizogony to produce up to 32 invasive daughter cells called the merozoites. Following their release from the host cell, these merozoites invade other erythrocytes and continue the intraerythrocytic life cycle.

A defining feature of apicomplexan parasites including the *Plasmodium* is the organelle Inner Membrane Complex (IMC) which are flattened membranous vesicles beneath the plasma membrane (PM). In *Plasmodium*, the IMC is present in the invasive or motile stages such as the merozoites, ookinetes, and sporozoites of all *Plasmodium*, as well as in the male gametocytes of human pathogen *P. falciparum* [2, 3]. In the asexual cycle of the *Plasmodium*, the biogenesis of the IMC begins at the early schizont stage after organelle duplication in the cytoplasm and several rounds of genome replication within the intact nucleus [4]. Allocation and packaging of nuclei and organelles into daughter cells are achieved by cytokinesis, in which the PM and the extending IMC coordinately invaginate and surround each daughter haploid merozoite [5]. As a result, the pellicle of merozoite is composed of single membrane of PM, closely aligned double membranes of the IMC, and 2-3 subpellicular microtubules (SPMT) associated with the IMC [6]. After invasion into a new erythrocyte, the IMC dissembles at the early ring stage [5]. The IMC is best recognized as the platform for attaching the actomyosin motor complex-glideosome (occupying in the space between PM and IMC) responsible for parasite invasion and motility [7, 8]. It also serves to maintain the cell shape and rigidity of the merozoite [9]. The cytoplasmic side of IMC is associated with a rigid meshwork composed of several families of proteins including alveolins [10], which is important for IMC-SPMT interconnection.

To understand the role(s) of the IMC in the parasite development, obtaining the complete list of protein components of the IMC is important. However, systematic proteomic analyses on the IMC protein composition have not been reported due to the difficulty in separating the IMC from other membranes, such as the PM. So far, a limited number of IMC and IMC-associated proteins have been identified, by either candidate gene strategy or isolating the interactors of IMC protein. Known IMC proteins include GAP45 (glideosome-associated protein 45) [11], GAP40 [12], GAP50 [13], MTIP (myosin A tail domain interacting protein)[14], MyoA [14], ECL1 [15], GAPM1 (GAP with multiple-membrane spans 1), GAPM2, and GAPM3 [16], as well as the alveolin proteins IMCp, IMC1c, IMC1e, IMC1f, IMC1g [3], and ISP3 [17]. In addition, CDPK1 (calcium-dependent kinase 1) and PhIL1 (Photosensitized INA-Labeled protein 1) were also reported to reside in the IMC of schizonts [18, 19]. BCP1, MORN1, and CINCH, components of the basal complex, a sub-compartment of the IMC at the posterior extending edge, were also recently identified [20]. Remarkably, most of the known IMC proteins were refractory to gene deletion, suggesting an essential function in the development of asexual blood stage [5]. Among the IMC proteins, GAP45 and CDPK1 have been studied extensively. CDPK1 plays a key role in early schizont development as its depletion or inhibition causes parasite arrest at the early schizonts [18, 21]. On the other hand, GAP45 is essential for merozoite invasion [11]. Despite great efforts in IMC research, many questions still remain regarding the IMC components and their function in schizogony. How many proteins are there in IMC? What determines IMC protein localization?

Enzyme-catalyzed proximity labelling (PL) coupled with mass spectrometry (MS) offers an alternative approach for proteome discovery [22]. BioID is an engineered bacterial biotin ligase adapted for proximity-based biotinylation of proteins in living cells [23]. The proteins covalently labeled with biotin can be isolated by streptavidin-biotin affinity purification followed by MS analysis. BioID has been used to identify the protein components of complexes and organelles in different model organisms [24]. In the *Plasmodium*, BioID-based PL had also generated organelle- and vesicle-specific proteins or proteomes, including those of the gametocyte-specific osmiophilic bodies of *P. berghei*, the blood stage parasitophorous vacuolar membrane of *P. berghei* and *P. falciparum*, the apicoplast of *P. falciparum*, and the IMC and apical annuli proteins of *P. falciparum* [25-30]. These analyses have led to the functional discovery of previously

undescribed proteins, providing new insights in the organelle biology of malaria parasites. However, BioID requires parasite exposure to biotin over a long period (18-24 h), which are not ideal or feasible for certain developmental stages with a short life span. In addition, BioID does not work well at temperatures below 37°C [31, 32], rendering its application to the mosquito stages of *Plasmodium* unsuitable. Recently, a new biotin ligase TurboID was developed by directed evolution [33]. Compared to BioID, TurboID is faster and can work under a broader range of temperature [33]. So far, the application of TurboID in the *Plasmodium* has not been reported.

In this study, we applied TurboID-proximity labeling and quantitative MS to obtain a proteome of the IMC in the schizonts of rodent malaria parasite *P. yoelii*. IMC targeting was achieved by fusing TurboID with the N-terminal 20 residues of ISP1, a known IMC resident protein. A collection of 300 proteins were identified as candidate IMC and IMC-associated proteins, of which 83 are potentially palmitoylated. We further demonstrated DHHC2 as a master IMC palmitoyl-acyl-transferase which plays a critical role in schizont segmentation and merozoite invasion by regulating the IMC localization of CDPK1 and GAP45 via palmitoylation.

Results

Biotin-labelling of *Plasmodium* proteins by TurboID ligase

To test the activity of the TurboID ligase relative to the BioID ligase for PL of malaria parasites, we fused a hemagglutinin (HA) tag to the N-terminus of each ligase (Fig S1A). These ligases were episomally expressed in the asexual blood stages of *P. yoelii* under the promoter of the *isp3* gene (Fig S1A), a gene that is highly transcribed in the schizonts [34]. Immunoblot detected comparable BioID and TurboID expressions in the asexual blood stages (Fig S1B). Different from an automatous rupture of mature schizonts of the *in vitro* cultured *P. falciparum*, the *P. yoelii* schizonts displayed an arrest in rupture after maturation in the *in vitro* condition, which permits PL of mature schizonts. The schizonts expressing each ligase were incubated with 100 µM biotin at 37°C for different time (0.25, 1, 3, and 18 h). Immunoblot using streptavidin-HRP detected robust protein biotinylation in the cell extracts of TurboID-parasites as early as 0.25 h after biotin incubation (Fig S1C). In contrast, protein biotinylation in the

BioID-parasites appeared at a low level at 3 h and reached a high level at 18 h (Fig S1C). To confirm these results, dot blot experiments were performed using streptavidin-HRP and similar results were observed (Fig S1D). Next we tested the temperature compatibility of the two ligases for PL in the parasites. BioID- and TurboID-schizonts were incubated for 18 and 3 h respectively, with 100 µM biotin at different temperatures (4, 22, 30, and 37°C). Biotin-incubated parasites stained with fluorescently conjugated streptavidin revealed that both ligases had similar labelling activity at 30 and 37°C (Fig S1E and F). Notably, only TurboID retained its activity at 22°C (Fig S1E and F). We further performed dot blots using streptavidin-HRP and obtained similar results (Fig S1G). These results indicate that TurboID is active at temperatures lower than 37°C, a temperature required for BioID to be fully functional. We also tested TurboID-mediated PL in the ookinetes, a mosquito stage of parasites with a preferential living temperature at 22°C. Cultured ookinetes from the BioID- and TurboID-parasites were incubated for 18 or 3 h respectively, with 100 µM biotin at 22°C. Co-staining with the fluorescently conjugated streptavidin and anti-HA antibody detected cytosolic protein biotinylation only in the TurboID-ookinetes when exogenous biotin was added (Fig S1H). Compared with BioID, TurboID allowed more robust PL of proteins in the living parasites with shorter biotin incubation time and is less temperature sensitive.

Detection of IMC proteins using TurboID labelling and quantitative mass spectrometry

Next we applied TurboID for PL of the IMC to identify new IMC proteins in the schizonts. The HA-tagged TurboID was fused with an IMC signal peptide, the N-terminal 20 residues of ISP1 (Tb-IMC) [17, 35] (Fig S2A). The HA-tagged TurboID alone (Tb-cyto) served as a control to indicate non-specific biotinylation (Figure 1A and Fig S2A), permitting specific identification of IMC and IMC-associated proteins. Both ligases (Tb-IMC and Tb-cyto) were driven by the promoter of gene *isp3* and episomally expressed in the asexual blood stages (Fig S2B). As expected, the Tb-IMC ligase dominantly co-localized with the IMC protein GAP45 in the IMC (Fig S2C). The schizonts expressing Tb-IMC, Tb-cyto, or empty vector (EV: construct without ligase

gene) were purified and treated with 100 μM biotin at 37°C for 3 h. Both immunoblot and dot blot assays using streptavidin-HRP detected increased biotinylation in cell extracts in the presence of biotin from the Tb-IMC and Tb-cyto schizonts, but not from the EV group (Figure 1B and Fig S2D). Furthermore, parasites stained with fluorescent-conjugated streptavidin (SA-488) and anti-HA antibody exhibited an IMC distribution (surrounding daughter merozoites) of biotinylated proteins, which co-localized with ligase in Tb-IMC schizonts. The biotinylated proteins and the ligase displayed cytosolic distribution in the Tb-cyto schizonts, while scarce signal was detected in the EV schizonts (Figure 1C and Fig S2E). Therefore, the Tb-IMC enables the PL of IMC in the living schizonts.

To further confirm that the IMC or IMC-associated proteins were the primary targets of biotin labeling in the Tb-IMC schizonts, the protein extracts were subjected to streptavidin pull-down, followed by immunoblot assays. As expected, cis-biotinylation of the Tb-IMC ligase was detected and the IMC protein GAP45 was enriched in the pull-down fraction (Fig S2F). In contrast, the proteins of other organelles, including the MSP1 (PM), Erd2 (Golgi marker), BiP (ER marker), and histone H3 (nucleus) were not detected (Fig S2F). Three biological replicates were prepared from the Tb-IMC and Tb-cyto schizonts, and the streptavidin-affinity purified proteins from cell extracts were subjected to proteomic analyses by SWATH-MS, a data-independent acquisition based quantitative MS method [36, 37]. The numbers of identified proteins with at least two independent peptides were comparable between the Tb-IMC (replicate 1:1964 hits, replicate 2:1995 hits, and replicate 3:1986 hits) and Tb-cyto schizonts (replicate 1:1970 hits, replicate 2:1946 hits, and replicate 3:1948 hits). Correlation analyses of changes in protein abundance demonstrated good reproducibility among biological replicates (Fig S2G). Quantitative MS yielded 488 enriched proteins with high confidence (an adjusted P value < 0.05) in the Tb-IMC compared to the Tb-cyto schizonts (Figure 1D and Fig S2H).

Genes coding for IMC proteins display transcription peak at late schizont and merozoite

during *P. falciparum* asexual replication cycle [38]. To further filter potential IMC proteins, we discriminated the 488 Tb-IMC interacting proteins by comparative analyses of their transcription pattern based on a *P. berghei* transcriptome dataset [34], thus narrowing the candidates to 300 proteins (Figure 1D, Fig S2H, Table S1). These 300 Tb-IMC proximal interactors included many known IMC or IMC-associated proteins, including GAP40, GAP45, GAP50, MTIP, MyoA, ELC, GAPM1, GAPM2, GAPM3, IMCp, IMC1c, IMC1e, IMC1f, IMC1g, ISP3, BCP1, MORN1, CINCH, CDPK1, PhIL1, DHHC1 and DHHC2 (Figure 1E and F). The homologs of these proteins have displayed an IMC or IMC-like localization in the *Plasmodium*, or have been shown to interact or associate with IMC protein baits using immunoprecipitation assay in previous studies [16, 18, 39-43]. Therefore, the IMC and IMC-associated proteins were enriched in the list of 300 Tb-IMC interacting proteins, suggesting reliable data quality generated by TurboID and quantitative MS.

Predicted functional profile of Tb-IMC interacting proteins

To further gain functional insights into the 300 Tb-IMC interacting proteins, we cross-referenced these proteins with other *Plasmodium* datasets. First, the Tb-IMC proximal interactors were significantly enriched for interactions using Search Tool for Retrieval of Interacting Genes/Proteins (STRING) [44], a database of known and predicted physical and functional protein-protein interactions. Notably, these proteins were segregated into two distinct subgroups (I and II) (Figure 1E and F). The subgroup I contained 152 proteins while the subgroup II contained 148 proteins. Most of known IMC or IMC-associated proteins were clustered into the subgroup I. In contrast, many annotated ER/Golgi secretory- or vesicle trafficking-related proteins were clustered into the subgroup II (Figure 1E and F). Second, gene ontology (GO) analysis was performed to further discriminate the proteins in subgroup I and II (Fig S3). Interestingly, the subgroup II was highly enriched with the GO terms, including the vesicle-mediated transport (40 proteins), vesicle fusion (11 proteins), ER to Golgi vesicle-mediated transport (13 proteins), Golgi vesicle transport (20 proteins) (Fig S3, biological process panel), and SNARE complex (14 proteins), endosome membrane (9 proteins), late

endosome (7 proteins), and endocytic vesicle (16 proteins) (cellular component panel), while the subgroup I was mainly assigned with the GO terms, like the inner membrane pellicle complex (22 proteins) (cellular component panel), protein lipidation (10 proteins) (biological process panel), and palmitoyltransferase activity (6 proteins) (molecular function panel). The IMC arises de novo from ER/Golgi-derived material via vesicular trafficking and membrane fusion in the schizonts of each replication cycle of the parasite [41, 45-47]. Detection of the subgroup II enriched with vesicular trafficking and membrane fusion effectors agrees with the notion of the ER/Golgi-derived IMC biogenesis. In addition, subgroup I and II within the Tb-IMC interacting proteins may reflect the tight and dynamic association between IMC organelle and endomembrane system in the schizont development.

Validation of the candidate IMC proteins

To assess whether the identified proteins are indeed localized in the IMC, 22 candidates were selected among the 300 Tb-IMC interacting proteins for subcellular localization analysis (Figure 2A). Among these proteins, the orthologues of 8 proteins including PY17X_ 0314700 (CDPK1), PY17X_0617900 (CDPK4), PY17X_1440500 (PKAr), PY17X_0839000 (PKAc), PY17X_1420600 (Rab11A), PY17X_1462100 (MTIP), PY17X_0206000 (PhIL1), and PY17X_0525300 (GAPM2) have been experimentally validated to be IMC-residing or association in the schizonts of *P. berghei* or *P. falciparum* [16, 18, 19, 40, 48-51], while IMC localization or association of the 14 other candidates (PY17X_0207400, PY17X_0312400, PY17X_0417300, PY17X_0418000, PY17X_0812700, PY17X_0917100, PY17X_1131200, PY17X_1139700, PY17X_1220300, PY17X_1348200, PY17X_1359500, PY17X_1411000, PY17X_1441500, and PY17X_1453100) (Figure 2B) have not been well characterized in the *Plasmodium*. Each candidate gene was tagged with a 6HA at the N- or C-terminus and driven by the promoter of gene *isp3* for episomal expression in the asexual blood stages. Immunoblot assays were used to detect each protein, all displaying a band fitting their expected molecular weight (Fig S4A). As expected, immunofluorescence assays (IFA) showed clear co-localization of the 8 known proteins (CDPK1, CDPK4, PKAr,

PKAc, Rab11A, MTIP, PhIL1, and GAPM2) with the IMC marker GAP45 (Fig S4B). Among the 14 newly characterized candidates, 11 of them (PY17X_0312400, PY17X_0418000, PY17X_0812700, PY17X_1131200, PY17X_1139700, PY17X_1220300, PY17X_1348200, PY17X_1359500, PY17X_1411000, PY17X_1441500, and PY17X_1453100) displayed the IMC or IMC-like pellicle localization (Figure 2C), while 3 other candidates (PY17X_0207400, PY17X_0417300, and PY17X_0917100) did not. Collectively, we confirmed the IMC or IMC-like localization of 19 proteins from the 22 candidates in the *P. yoelii* schizonts.

Palmitoylation of IMC proteins and regulation of localization

While a growing number of IMC proteins were discovered, their localization determinants remain incompletely known. Protein palmitoylation is a reversible lipid modification that facilitates protein attachment to the plasma and organelle membranes [52]. Previous studies have shown that palmitoylation is important for the binding or targeting of proteins to IMC in the *Plasmodium* [17, 35]. We speculated that certain IMC proteins use lipid moieties for IMC membrane attachment. Interestingly, we observed a significant enrichment of the biological-process term of protein lipidation (GO: 0006497) in the Tb-IMC interacting proteins (Figure 3A and Fig S3). Three palmitoyl-S-acyl-transferases (PAT) including DHHC1, DHHC2, and DHHC7, were enriched (Figure 3A), implying a role of these PATs for palmitoylation of the IMC proteins.

To identify IMC proteins with palmitoylation, we examined a collection of 494 palmitoylated proteins previously detected in the schizonts of *P. falciparum* [53]. Among the 300 *P. yoelii* Tb-IMC interacting proteins identified in this study, 83 proteins (28%) have orthologs that are palmitoylated in the *P. falciparum* (Figure 3B and Table S2). Importantly, these 83 proteins includes GAP45 and ISP3, whose palmitoylations have been experimentally validated [17, 53], and CDPK1, GAP50, IMC1g, and IMC1c, which are predicted to be palmitoylated. Out of these 83 proteins, we assessed 4 (CDPK1, GAP45, ISP3, and a newly identified IMC protein PY17X_1411000) for their

277 palmitoylation using resin-assisted capture of acylated proteins (Acyl-RAC) method
278 [54]. Palmitoylation was confirmed in these 4 proteins in *P. yoelii* schizonts (Figure 3C)
279 while PhIL1, an IMC protein not in the list of 83 proteins, did not display palmitoylation
280 (Figure 3C). To further confirm palmitoylation, the schizont culture was treated with
281 100 μM 2-bromopalmitate (2-BP), an inhibitor of protein palmitoylation. We observed
282 markedly reduced palmitoylation of CDPK1, GAP45, and ISP3 in the 2-BP treated
283 schizonts (Figure 3D). Notably, CDPK1, GAP45, and 1411000 lost their IMC
284 localization and were found in the cytosol after 2-BP treatment (Figure 3E). As a control,
285 the PM localization of merozoite surface protein MSP1 was unaffected. Fractionation
286 of schizont protein extracts (Figure 3F) revealed that CDPK1, GAP45, and 1411000
287 were mainly present in the heavy fraction, in agreement with the IMC membrane
288 association of these proteins. However, these proteins were mostly detected in the light
289 fraction after 2-BP treatment, suggesting their distribution alterations after losing the
290 palmitoylation. Together, these results suggest that palmitoylation may exist in a
291 relatively high proportion of the IMC proteins and that it is important for subcellular
292 localization of certain IMC proteins including CDPK1, GAP45, and 1411000.
293
294 **DHHC2 is an IMC-residing palmitoyl-S-acyl-transferase in schizonts**
295 Next, we searched for the PATs that catalyze the palmitoylation of IMC residing
296 proteins in the schizonts. 11 putative PATs (named DHHC1–11) were predicted in the
297 genomes of rodent malaria parasites [39]. Quantitative reverse transcription-PCR (qRT-
298 PCR) analysis revealed that the *P. yoelii dhhc2* displayed the highest mRNA level in
299 the schizonts (Figure 4A). The mRNA levels of these *P. yoelii dhhc* genes were
300 positively correlated ($R^2 = 0.94$) with the transcription profiles of their orthologs in *P.*
301 *berghei* determined via RNA-seq [34] (Figure 4A). Furthermore, we analyzed the
302 localization of the 11 *P. yoelii* endogenous PATs individually in the schizonts of
303 transgenic strains previously generated [17]. Out of the 11 PATs, only DHHC1 and
304 DHHC2 displayed clear IMC localization in the schizonts with a stronger IFA signal
305 for DHHC2 (Figure 4B and Fig S5A). Immunoblot analysis of protein extracts from the
306 same number of schizonts of the endogenously tagged *dhhc2::6HA* and *dhhc1::6HA*

307 parasites revealed approximately 5-fold higher level of DHHC2 than DHHC1 (Figure
308 4C). Interestingly, DHHC2 but not DHHC1 displayed an interrelation with several IMC
309 proteins, including CDPK1 and GAP45, in a STRING analysis which predicts the
310 likelihood of protein-protein interaction (Fig S5B). The IMC localization of DHHC2
311 was confirmed in two independent strains *6HA::dhhc2* and *dhhc2::4Myc*, whose
312 endogenous DHHC2 was tagged with a N-terminal 6HA and C-terminal 4Myc tag,
313 respectively (Figure 4D). Immunoblot analyses of the membrane and cytoplasmic
314 fractions of schizont lysates also revealed that DHHC2 was mainly detected in the
315 membrane fraction (Figure 4E). As a control, merozoite PM protein MSP1 was detected
316 in the membrane fraction while the cytosolic protein GAPDH was in the cytoplasmic
317 fraction (Figure 4E).
318
319 To investigate the expression dynamics of DHHC2 during parasite development, early
320 and later stages of intraerythrocytic *dhhc2::6HA* parasites were isolated using the
321 Nycodenz gradient centrifugation. Immunoblot showed that DHHC2 is highly
322 expressed in the late trophozoites and schizonts, but not in the rings or early
323 trophozoites (Figure 4F). IFA also revealed DHHC2 signal in the early and mature
324 schizonts and free merozoites (Figure 4G). These observations were independently
325 confirmed in another strain *gfp::dhhc2*, in which endogenous DHHC2 was tagged with
326 a N-terminal GFP (Figure 4H). The expression dynamics of DHHC2 is consistent with
327 the IMC biogenesis in the schizonts. Using the Airyscan microscopy, we observed clear
328 co-localization between DHHC2 and GAP45 in both early and mature schizonts (Figure
329 4I). Interestingly, both proteins were found as separate dots at the periphery of the intact
330 nucleus in the early schizonts (Figure 4I), suggesting that IMC arises de novo at
331 multiple points at or close to the nucleus. Together, these results indicate that DHHC2,
332 as an IMC-residing PAT, is expressed throughout the IMC biogenesis in the schizonts
333 of *P. yoelii*. (Figure 4J)
334
335 **DHHC2 is essential for the asexual blood stage development in mice**
336 DHHC2 has been suggested to play an essential role in the asexual blood stage

development of the parasites since no viable mutant clone was obtained using either the conventional or Cas9-based knockout strategies in the *P. yoelii* and *P. berghei* [17, 55]. To explore the functions of DHHC2, we applied an Auxin-inducible degron (AID)-based protein degradation system in the *P. yoelii* transgenic strain *Tir1* [56], which allows depletion of the target protein fused to a miniAID (mAID) motif with the aid of the plant hormone auxin (Indole-3-acetic acid, IAA). The N-terminus of the endogenous *dhhc2* locus was tagged with the sequence encoding mAID::2HA in the *Tir1* strain, generating the *mAID::dhhc2* clone (Fig S6A). This parasite displayed normal proliferation during asexual blood stages and the fusion protein mAID::DHHC2 exhibited IMC localization in the schizonts (Fig S6B), indicating no detrimental effect of mAID tagging on DHHC2 localization and function. IAA treatment (1 mM for 3 h) of the *mAID::dhhc2* schizonts efficiently depleted the mAID::DHHC2 protein (Fig S6C). To determine whether IAA itself affects parasites development *in vivo*, mice infected with the 17XNL parasite were injected intraperitoneally with 200 mg/kg/day IAA or vehicle (DMSO) for 3 consecutive days. The *in vivo* parasitemia increased at an indistinguishable rate in both groups (Fig S6D), indicating no notable effect of IAA on parasite proliferation in mice. Next, we tested whether the parasite mAID::DHHC2 protein could be depleted in mice. The mice with ~10% parasitemia of the *mAID::dhhc2* parasite were injected intraperitoneally with IAA once and the parasite-infected red blood cells were collected for immunoblot at 1 and 3 h after IAA injection (Fig S6E). The mAID::DHHC2 protein was significantly reduced in the parasites from IAA-treated mice, indicating successful mAID::DHHC2 degradation by IAA (Fig S6E). As a control, the IAA treatment had little effect on the 6HA::DHHC2 protein in the *6HA::dhhc2* parasite (Fig S6E).

To dissect the DHHC2 function *in vivo*, mice were infected with the *Tir1* or *mAID::dhhc2* schizonts which were pretreated with IAA or vehicle for 3 h *in vitro* to deplete DHHC2 (Figure 5A). From 12 h post infection, the parasitemia in mice infected with *Tir1* and *mAID::dhhc2* was monitored in parallel every 12 h. The parasitemia of *Tir1* increased at an equal rate after either IAA or vehicle pretreatment (Figure 5B, left

panel). However, the IAA-pretreated *mAID::dhhc2* parasite displayed delayed proliferation compared to the parasite pretreated with vehicle (Figure 5B, right panel). The parasite with IAA-pretreatment emerged in the mouse blood at 96 h post infection while the parasite with vehicle-pretreatment emerged at 36 h. Notably, continuation of DHHC2 depletion by another IAA injection (IAA+) at time of parasite infection resulted in complete suppression of *mAID::dhhc2* in mice (Figure 5B, right panel), while this treatment had no effect on the proliferation of *Tir1* (Figure 5B, left panel). These results provided a direct evidence that DHHC2 is essential for the asexual blood stage development in mice.

DHHC2 regulates schizont segmentation

Because DHHC2 is specifically expressed in the schizonts, we speculated that DHHC2 regulates schizont development. A mixture of early stage parasites (rings and early trophozoites) was purified using Nycodenz centrifugation and cultured for 12 h to mature schizonts using an *in vitro* culture method [57] (Figure 5C). We evaluated the effect of DHHC2 depletion on schizont development by counting the mature schizonts using Giemsa staining. The IAA-treated *Tir1* parasite developed to mature schizonts at a similar level as the vehicle-treated *Tir1* parasite, indicating no effect of IAA alone on the schizont development (Figure 5D and E). However, IAA treatment severely decreased the formation of mature schizonts in the *mAID::dhhc2* parasite (Figure 5D and E). Importantly, the treated *mAID::dhhc2* parasite had apparent nuclear replication but failed to segregate into individual merozoites. This result suggests arrest of schizont cytokinesis or segmentation after nuclear multiplication. In addition, treatment with the PAT inhibitor 2-BP resulted in no formation of mature schizonts in either *Tir1* or *mAID::dhhc2* parasites (Figure 5D and E), which is in agreement with the previous reports [53].

To further examine the defects within the schizonts, the *mAID::dhhc2* parasite was co-stained with the nuclear dye and an antibody against the merozoite surface protein MSP1, which coats the parasite PM of newly formed daughter merozoites after

segmentation [58]. Hoechst signals in the schizonts showed no notable difference between the IAA- and vehicle-treated groups (Figure 5F and G), indicating normal nuclear DNA multiplication in the DHHC2-deficient (IAA-treated) parasites. However, MSP1 staining revealed that the schizonts of DHHC2-deficient group had agglomerates of daughter cells that failed to separate (Figure 5F) while the schizonts of the vehicle control group exhibited normal morphology (Figure 5F). Expression and cleavage (from ~200 to 42 kD) of full length MSP1 have been used to indicate schizont maturation and merozoite ready-to-egress from erythrocytes [59, 60]. Consistent with an impaired schizont development, an immunoblot of the IAA-treated parasite showed reduced MSP1 expression and processing compared to the vehicle control (Figure 5H).

Next, using transmission electron microscopy (TEM), we examined the ultra-structure of the *mAID::dhhc2* schizonts produced after the 12 h *in vitro* maturation in the presence of the vehicle, IAA, or 2-BP. The daughter cells were normally segmented in the schizonts of the vehicle-treated group, forming fully separated daughter merozoites (Figure 5I). However, severe morphological defects occurred in the DHHC2-deficient parasites. Large daughter cell agglomerates were observed in the center of most schizonts although a few mononucleated daughter merozoites were formed (Figure 5I). This segmentation arrest resulted in significant fewer daughter merozoites in the DHHC2-deficient schizonts compared to the control (Figure 5J). Interestingly, we observed the incomplete IMC beneath the PM in some daughter merozoites and the agglomerates within the DHHC2-deficient schizonts (Figure 5I), suggesting no remarkable effect of DHHC2 depletion in the initial biogenesis of the IMC. In addition, the organelles including possible rhoptries or micronemes were observed in the large agglomerates of the DHHC2-deficient schizonts, suggesting normal biogenesis and development of these organelles but a defect in allocation of daughter merozoites during schizont segmentation. As a control, the 2-BP treatment completely blocked schizont segmentation (Figure 5I).

DHHC2 also controls merozoite invasion

Upon schizont maturation, merozoites egress from the erythrocyte to invade new erythrocytes. To investigate DHHC2 function in merozoite invasion, we collected the merozoites released from the mechanically disrupted mature schizonts, which undergo natural rupture in an extremely low efficacy under the *in vitro* condition for the *P. yoelii*. Released merozoites were capable of invading the erythrocytes in mice, indicative of merozoite's viability and activity. The merozoites collected from the IAA- or vehicle-treated schizonts were injected intravenously into mice and the number of the ring stage parasites indicative of successful invasion was counted by flow cytometry and light microscopy (Figure S7A). At 20 min post injection, the number of newly developed rings was significantly lower in the IAA-treated group compared with the vehicle-treated group (Figure S7B and C). As a control, the IAA treatment had no effect on merozoite invasion of the *Tir1* parasite (Figure S7 B and C). Taking all the results together, DHHC2 has an important function in both schizont segmentation and merozoite invasion, two processes during which the parasites possess IMC.

DHHC2 palmitoylates GAP45 and CDPK1

GAP45 and CDPK1 are essential for the asexual blood stage development of *P. falciparum* [11, 18, 21]. Additionally, palmitoylation regulates IMC targeting of these proteins in the schizonts and merozoites (Figure 3E). We speculated that DHHC2 exerts its function via palmitoylating GAP45 and CDPK1. To test this hypothesis, the palmitoylation and localization of GAP45 and CDPK1 were examined in the DHHC2-deficient schizonts after pretreating with IAA at 1 mM for 12 h. The palmitoylation level of GAP45 and CDPK1 was significantly reduced in the DHHC2-deficient schizonts compared to the vehicle control (Figure 6A). Notably, both GAP45 and CDPK1 lost their typical IMC localization in both the schizonts and the released merozoites of the DHHC2-deficient parasite (Figure 6C and D). In contrast, PhIL1 retained the IMC localization in the DHHC2-deficient parasite (Figure 6C), consistent with the fact that PhIL1 is not palmitoylated (Figure 4C). The distribution of MSP1 in the DHHC2-deficient schizonts was also unaffected (Figure 6C). In agreement with the changes in subcellular distribution of proteins by IFA, the detergent extraction-based

protein solubility assay also revealed that GAP45 and CDPK1 lost their membrane association upon the depletion of DHHC2 by IAA (Figure 6E).

Besides DHHC2, DHHC1 also displayed IMC localization in the schizonts although it is expressed at lower abundance (Figure 4B and C). To investigate whether DHHC1 also contributes to the palmitoylation of GAP45 and CDPK1, we generated the *dhhc1::mAID* parasite clone in which the C-terminus of endogenous DHHC1 was tagged with the mAID::HA module in the *Tir1* strain (Fig. S6A and B). IAA treatment depleted the DHHC1::mAID protein in the *dhhc1::mAID* schizonts (Fig. S6C), but had little impact on the palmitoylation level of GAP45 and CDPK1 (Figure 6B). These results indicated that DHHC2, but not DHHC1, contributes to the palmitoylation of GAP45 and CDPK1 in the schizonts.

To further confirm DHHC2 as the enzyme capable of palmitoylating GAP45 and CDPK1, we transfected constructs encoding HA-tagged human codon optimized DHHC2 (DHHC2-HA), GAP45 and CDPK1 into the human HEK293T cells. Indeed, the ectopically expressed GAP45 and CDPK1 could be palmitoylated by co-transfected DHHC2-HA, while the PAT catalytic-deficient mutant protein DHHC2/C128A-HA failed to palmitoylate GAP45 and CDPK1 (Figure 6F). As a control, the palmitoylation of co-transfected mouse CD36 protein, which was reported to be constitutively palmitoylated in HEK293T [61], was independent of *Plasmodium* DHHC2 (Figure 6F). The palmitoylation of GAP45 and CDPK1 was also significantly reduced in HEK293T culture treated with inhibitor 2-BP (Figure 6G). These results in human cells replicate the observations of DHHC2 activity in the *Plasmodium* schizonts and demonstrate the ability of DHHC2 to palmitoylate GAP45 and CDPK1.

Residues for palmitoylation in GAP45 and CDPK1

To identify the residue(s) of palmitoylation in GAP45, we used an online software CSS-Palm (csspalm.biocuckoo.org) for prediction, which generated 6 candidate cysteines (C5, C140, C156, C158, C169, and C172) (Figure 7A). To test them, we initially

generated 4 constructs expressing HA-tagged GAP45, each with a single or double cysteine-to-alanine mutations (C5A, C140A, C156A/C158A, and C169A/C172A) (Figure 7A, Fig S8A and B). These constructs were episomally expressed in the schizonts. Only the C140A mutant displayed the IMC localization similar to wildtype (WT) GAP45; other mutants (C5A, C156A/C158A, and C169A/C172A) lost the IMC localization (Figure 7B). These results suggest that these cysteines (C5, C156 and/or C158, C169 and/or C172) are critical for IMC targeting of GAP45 and might be the residues for modification. Indeed, the Acyl-RAC assay detected significantly decreased palmitoylation of GAP45 in the C5A, C156A/C158A, and C169A/C172A mutants, but not the C140A mutant. Thus, for GAP45, there is an association between IMC localization and palmitoylation. Additionally, the degree of palmitoylation was further reduced in the triple cysteine mutants (C5A/C156A/C158A and C5A/C169A/C172A) relative to the single and double mutants (Figure 7C).

In CDPK1, two cysteines (C3 and C252) were predicted as the potential residues for palmitoylation (Figure 7D). Using the same approach, we found that only the C3A mutation caused a complete loss in both protein palmitoylation and IMC targeting of CDPK1 in the schizonts while the C252A mutation had no effect (Figure 7E-F), suggesting C3 as the critical residue for protein palmitoylation and IMC targeting of CDPK1 in schizonts. Interestingly, the cysteine residues C5, C156, C158, C169, and C172 of GAP45 and C3 of CDPK1 are evolutionarily conserved among different *Plasmodium* species (Fig S8A and C). Together, these results suggest that C5, C156, C158, C169, and C172 of GAP45 and C3 of CDPK1 are residues for palmitoylation which direct IMC targeting of the proteins in schizonts.

Palmitoylation in GAP45 and CDPK1 is essential for parasite viability

Lastly we asked whether the palmitoylation in GAP45 and CDPK1 is essential for protein function and thus parasite viability. The above cysteine to alanine mutation experiments indicated that the palmitoylation of the N-terminal cysteine (C5 in GAP45 and C3 in CDPK1) is required for the correct IMC targeting of proteins. We attempted

517 to replace the C5 with alanine in the endogenous GAP45 of 17XNL parasite. A 742 bp
518 DNA donor template containing the nucleotide substitution was used for homologous
519 replacement (Fig S9C). Seven sgRNAs were designed for guiding the Cas9 complex to
520 the target DNA. After three independent transfections with each of these seven
521 Cas9/sgRNA plasmids, we failed to obtain the GAP45 C5A mutant parasites. In contrast,
522 a control mutant parasite clone GAP45 C5C was generated with a silent mutation still
523 encoding C5 (Fig S8E). Using the same approach, we attempted to replace the C3 with
524 A in the endogenous CDPK1 of 17XNL parasite (Fig S9C). Similarly, only mutant
525 parasite clones with CDPK1 C3C, but not CDPK1 C3A, were generated (Fig S8F).
526 Together, these results suggest that palmitoylation of C5 in GAP45 and C3 in CDPK1
527 is essential for protein function and parasite viability in the asexual blood stage
528 development.
529

530 ## Discussion

531 In this study, we attempted a proteome analysis of IMC in the schizonts using the biotin
532 ligase TurboID-mediated PL. Besides abundant proteins relatively easily detected by
533 conventional immunoprecipitation, PL enables detection of proteins with weak or
534 transient interactions. TurboID achieved satisfactory biotinylation in 1 h, which is much
535 shorter than the 18 h needed by the BioID. To our knowledge, this is the first application
536 of TurboID-based PL in the *Plasmodium*. We obtained a list of 300 Tb-IMC interacting
537 proteins in the schizonts of *P. yoelii*. Among these proteins, 297 have orthologs in the
538 *P. falciparum* (Table S1), suggesting a conserved protein composition of IMC in the
539 schizonts of rodent and human malaria parasites. Although the collection of 300
540 proteins may contain some false positives, two lines of evidence suggest good reliability
541 of this IMC proteome. Firstly, about 50 IMC or IMC-associated proteins have been
542 identified in the *Plasmodium* to date [5, 30]. Among these, 30 proteins (60%) have
543 orthologs included in the Tb-IMC interacting proteins (Table S1). The absence of
544 certain known IMC or IMC-associated proteins in the collection of Tb-IMC interacting
545 proteins may attribute to the following reasons: restricted labeling radius of TurboID,

lack of lysines for biotinylation, sterically inaccessibility of proteins by TurboID, or protein expression in other parasite stages [62]. Secondly, subcellular localization analysis of 22 candidates confirmed IMC localization of 8 known and 11 previously undescribed proteins. The localization results strongly suggest a predominantly IMC localization of the proteins tested, although the precise localization at the parasite plasma membrane or subpellicular microtubules cannot be differentiated because of close proximity between IMC and these structures. Exact localization of these proteins at the parasite pellicle need to be determined in the future using other methods, such as super resolution imaging, immunoelectron microscopy, or split green fluorescent protein. We noted that Wichers *et al* recently explored an IMC proteome in asexual blood stages of *P. falciparum* with BioID using PhIL1 as the bait [30]. Of the 225 PhIL1-interacting protein candidates, the orthologs of 37 proteins are listed among the 300 Tb-IMC interacting proteins in our study (Table S1). We speculate that the differences in protein quantity and depth by proximity labeling are probably attributed to the species of biotin ligase, expression abundance of ligase, and the bait strategy.

PL experiments could produce a considerable number of false positives if proper controls are not included for ratiometric or statistical analysis [24]. In a rational design, the PL enzyme is fused to the protein bait of interest while the PL enzyme alone works as a reference control [24]. To achieve the PL of IMC, the TurboID ligase is fused to a signal peptide (N-terminal 20 aa of ISP1) [17], directing the IMC targeting of ligase (Tb-IMC) through the ER/Golgi secretary pathway. It is worth noting that the cytoplasm-facing feature of Tb-IMC ligase may prevent the detection of proteins in the IMC lumen. Background levels of ligase activity are set by a ligase not fused to the signal peptide. This ligase (Tb-cyto), as a spatial reference control, would not enter the ER/Golgi secretory pathway but instead stays in the cytosol. Therefore, the Tb-IMC likely measures both interactions with the IMC proteins and interactions with the secretory pathway. Indeed, the 300 Tb-IMC interacting proteins were segregated into two distinct subgroups based on interaction network (Figure 1E). Most of known IMC or IMC-associated proteins were clustered into the subgroup I. In contrast, the subgroup

II included many ER/Golgi secretory pathway-related proteins. The major role of the subgroup I proteins is likely in IMC function while the major role of the subgroup II proteins is likely in the secretory pathway. It is possible that some Tb-IMC interacting proteins may have roles in both IMC and secretory pathway. Detection of the subgroup II proteins in this study provided another independent evidence supporting the IMC formation from the ER/Golgi-derived secretory system. In addition, concomitant capture of subgroup I and II as the Tb-IMC interacting proteins may reflect the tight and dynamic association between IMC organelle and endomembrane system in the schizont development.

The list of increased IMC proteins allowed us to investigate the localization determinant(s) of IMC proteins which had remained unclear. Several mechanisms underlying IMC targeting have been proposed, including vesicle-mediated transporting of proteins containing a signal peptide, IMC membrane trapping of proteins with lipid modification, protein motif (alveolin repeats)-mediated IMC localization, and protein-protein interaction for IMC targeting [3]. Palmitoylation is a post-translation modification in which a cysteine residue undergoes a reversible lipid modification, regulating localization and function of target proteins [63]. Previous studies have implied that palmitoylation mediates the binding or trafficking of proteins to the IMC [17, 35]. In *T. gondii,* many glideosome-associated proteins were also palmitoylated [64]. Interestingly, out of the 300 *P. yoelii* Tb-IMC interacting proteins, 83 (28%) have orthologs of the *P. falciparum* palmitoylated proteins in the schizonts of [53]. These 83 proteins include GAP45 and ISP3 with validated palmitoylation and CDPK1, GAP50, IMC1g, and IMC1c with predicted palmitoylation. These results imply that a high proportion of IMC proteins are palmitoylated. Palmitoylation of these proteins may be critical for their localization and function. Interaction of these palmitoylated IMC proteins with other non-palmitoylated proteins may also mediate the IMC localization of the latter.

11 putative PATs (DHHC1–11) are encoded in the genomes of rodent malaria parasites

606 while there are 12 PATs (DHHC1-12) in *P. falciparum* [39]. So far, viable mutant clones
607 were obtained for only DHHC3, DHHC5, DHHC9, and DHHC10 in previous knockout
608 attempts [65-67], suggesting other PATs (DHHC1, DHHC2, DHHC4, DHHC6,
609 DHHC7, DHHC8, DHHC11, and DHHC12) may be essential for the asexual blood
610 stage development. However, the association of these PATs with IMC has not been
611 investigated in the schizonts. In this study, DHHC2 and DHHC1 are among the 300 Tb-
612 IMC interacting proteins and both displayed clear IMC localization in the schizonts.
613 Protein abundance assays and STRING analysis suggested that DHHC2 is likely the
614 main mediator of palmitoylation of the IMC proteins in the schizonts. To determine if
615 DHHC2 contributes to parasite development *in vivo*, we developed a method for
616 investigating its function in the infected mice. Induced depletion of DHHC2 resulted in
617 a complete growth arrest of the engineered strain *mAID::dhhc2* in mice in an IAA
618 dosage-dependent manner, confirming the essentiality of DHHC2 in the asexual blood
619 stage. In *in vitro* culture, we observed a significant decrease, but not complete ablation
620 of mature schizont formation in DHHC2-depleted parasites. Most parasites were
621 arrested at a stage earlier than the mature schizont due to defective segmentation or
622 cytokinesis. The defect in asexual blood stage development *in vivo* and *in vitro* caused
623 by the loss of DHHC2 was associated with impairment of IMC localization of certain
624 IMC proteins. Indeed, among the 83 potentially palmitoylated IMC proteins, our
625 analysis validated CDPK1 and GAP45 as substrates of DHHC2, but not DHHC1. Aside
626 from CDPK1 and GAP45, other IMC protein substrates palmitoylated by DHHC2
627 remain to be validated. We previously reported that DHHC2 is critical for parasite
628 development during the zygote-to-ookinete morphogenesis in the mosquito, and
629 DHHC2 palmitoylates ISP1 and ISP3 for their attachment to the IMC to facilitate
630 connection between the IMC and the SPMT [17]. Therefore, DHHC2 plays critical roles
631 in IMC targeting of many proteins at multiple developmental stages.
632
633 Compared to the reduction in the *mAID::dhhc2* schizonts caused by IAA treatment, the
634 treatment with 2-BP, a broad-spectrum inhibitor of protein palmitoylation, resulted in
635 no formation of mature *mAID::dhhc2* schizonts (Figure 6D and E). The effects of IAA

636 are specific to the mAID-fused DHHC2 in the *mAID::dhhc2* schizonts, whereas 2-BP
637 could inhibit protein palmitoylation mediated by DHHC2 and other PATs, including
638 DHHC1. We suspect that the IMC-residing DHHC1 is also essential for schizont
639 development, but its precise roles and substrate proteins also awaits investigation in the
640 future.
641
642 Besides the PATs DHHC2 and DHHC1, several kinases including CDPK1, CDPK4,
643 and PKA, were also found among the Tb-IMC interacting proteins. CDPK1, CDPK4,
644 and PKA were further validated to localize at the IMC of *P. yoelii*, in accordance with
645 their orthologs' localization in *P. falciparum* [18, 48, 49]. CDPK1 has been reported to
646 be essential for schizont development. Both conditional knockdown and inhibition of
647 CDPK1 can arrest *P. falciparum* schizont development [18, 21], mimicking the
648 phenotypes of the DHHC2-depleted parasites in this study. Interestingly,
649 phosphoproteomic analysis revealed that the conditional knockdown of CDPK1 led to
650 the hypophosphorylation of several IMC and glideosome proteins, including GAP45,
651 MTIP, and PKA regulatory subunit (PKAr) [18, 49, 68, 69]. In this study, we found that
652 DHHC2-mediated palmitoylation is required for CDPK1 localization at IMC. Thus
653 palmitoylation and IMC localization are the prerequisites for CDPK1-mediated
654 phosphorylation of IMC proteins. Based on all available data, we speculated that once
655 the IMC biogenesis is initiated in early schizonts, DHHC2 is recruited to the nascent
656 IMC, possibly by an auto-palmitoylation mechanism [17]. However, DHHC2 seems
657 inessential for IMC biogenesis because the IMC seemed morphologically normal
658 despite DHHC2 depletion (Figure 5I). In contrast, DHHC2 palmitoylates certain
659 important proteins for their IMC localization in the developing schizonts and mature
660 merozoites. It has critical function in schizont cytokinesis and erythrocyte invasion.
661

662 ## Acknowledgments

663 This work was supported by the National Natural Science Foundation of China
664 (32170427, 31970387, 31872214), the Natural Science Foundation of Fujian Province

(2021J01028, 2019J05010), and the 111 Project sponsored by the State Bureau of Foreign Experts and Ministry of Education of China (BP2018017).

Author contributions

Q.PG. and W.X. generated the modified parasites, conducted the phenotype analysis, IFA assay, image analysis, TEM experiments, and biochemical experiments. Z.CQ. conducted the MS and data analysis. C.MY. and W.JX. generated the modified parasites. Y.J. and C.HT, supervised the work. Q.PG, L.J, C.HT, and Y.J. analyzed the data, W.N. revised the manuscript, and Y.J. wrote the manuscript.

Declaration of Interests

The authors declare no competing interests

References

1. Organization, W.H. (2019). World malaria report 2019. (Geneva: World Health Organization).
2. Morrissette, N.S., and Sibley, L.D. (2002). Cytoskeleton of apicomplexan parasites. Microbiology and molecular biology reviews : MMBR *66*, 21-38; table of contents.
3. Kono, M., Herrmann, S., Loughran, N.B., Cabrera, A., Engelberg, K., Lehmann, C., Sinha, D., Prinz, B., Ruch, U., Heussler, V., et al. (2012). Evolution and architecture of the inner membrane complex in asexual and sexual stages of the malaria parasite. Mol Biol Evol *29*, 2113-2132.
4. Matthews, H., Duffy, C.W., and Merrick, C.J. (2018). Checks and balances? DNA replication and the cell cycle in Plasmodium. Parasit Vectors *11*, 216.
5. Ferreira, J.L., Heincke, D., Wichers, J.S., Liffner, B., Wilson, D.W., and Gilberger, T.W. (2020). The Dynamic Roles of the Inner Membrane Complex in the Multiple Stages of the Malaria Parasite. Front Cell Infect Microbiol *10*, 611801.
6. Kono, M., Heincke, D., Wilcke, L., Wong, T.W., Bruns, C., Herrmann, S., Spielmann, T., and Gilberger, T.W. (2016). Pellicle formation in the malaria parasite. J Cell Sci *129*, 673-680.
7. Frenal, K., and Soldati-Favre, D. (2013). [The glideosome, a unique machinery that assists the Apicomplexa in gliding into host cells]. Med Sci (Paris) *29*, 515-522.
8. Harding, C.R., and Frischknecht, F. (2020). The Riveting Cellular Structures of Apicomplexan Parasites. Trends Parasitol *36*, 979-991.
9. Frenal, K., Dubremetz, J.F., Lebrun, M., and Soldati-Favre, D. (2017). Gliding motility powers invasion and egress in Apicomplexa. Nat Rev Microbiol *15*, 645-660.
10. Gould, S.B., Tham, W.H., Cowman, A.F., McFadden, G.I., and Waller, R.F. (2008). Alveolins, a new family of cortical proteins that define the protist infrakingdom Alveolata. Mol Biol Evol *25*, 1219-1230.

11. Perrin, A.J., Collins, C.R., Russell, M.R.G., Collinson, L.M., Baker, D.A., and Blackman, M.J. (2018). The Actinomyosin Motor Drives Malaria Parasite Red Blood Cell Invasion but Not Egress. mBio *9*.
12. Frenal, K., Polonais, V., Marq, J.B., Stratmann, R., Limenitakis, J., and Soldati-Favre, D. (2010). Functional dissection of the apicomplexan glideosome molecular architecture. Cell Host Microbe *8*, 343-357.
13. Bosch, J., Paige, M.H., Vaidya, A.B., Bergman, L.W., and Hol, W.G. (2012). Crystal structure of GAP50, the anchor of the invasion machinery in the inner membrane complex of Plasmodium falciparum. J Struct Biol *178*, 61-73.
14. Bergman, L.W., Kaiser, K., Fujioka, H., Coppens, I., Daly, T.M., Fox, S., Matuschewski, K., Nussenzweig, V., and Kappe, S.H. (2003). Myosin A tail domain interacting protein (MTIP) localizes to the inner membrane complex of Plasmodium sporozoites. J Cell Sci *116*, 39-49.
15. Green, J.L., Wall, R.J., Vahokoski, J., Yusuf, N.A., Ridzuan, M.A.M., Stanway, R.R., Stock, J., Knuepfer, E., Brady, D., Martin, S.R., et al. (2017). Compositional and expression analyses of the glideosome during the Plasmodium life cycle reveal an additional myosin light chain required for maximum motility. J Biol Chem *292*, 17857-17875.
16. Bullen, H.E., Tonkin, C.J., O'Donnell, R.A., Tham, W.H., Papenfuss, A.T., Gould, S., Cowman, A.F., Crabb, B.S., and Gilson, P.R. (2009). A novel family of Apicomplexan glideosome-associated proteins with an inner membrane-anchoring role. J Biol Chem *284*, 25353-25363.
17. Wang, X., Qian, P., Cui, H., Yao, L., and Yuan, J. (2020). A protein palmitoylation cascade regulates microtubule cytoskeleton integrity in Plasmodium. EMBO J *39*, e104168.
18. Kumar, S., Kumar, M., Ekka, R., Dvorin, J.D., Paul, A.S., Madugundu, A.K., Gilberger, T., Gowda, H., Duraisingh, M.T., Keshava Prasad, T.S., et al. (2017). PfCDPK1 mediated signaling in erythrocytic stages of Plasmodium falciparum. Nat Commun *8*, 63.
19. Saini, E., Zeeshan, M., Brady, D., Pandey, R., Kaiser, G., Koreny, L., Kumar, P., Thakur, V., Tatiya, S., Katris, N.J., et al. (2017). Photosensitized INA-Labelled protein 1 (PhIL1) is novel component of the inner membrane complex and is required for Plasmodium parasite development. Sci Rep *7*, 15577.
20. Morano, A.A., and Dvorin, J.D. (2021). The Ringleaders: Understanding the Apicomplexan Basal Complex Through Comparison to Established Contractile Ring Systems. Front Cell Infect Microbiol *11*, 656976.
21. Azevedo, M.F., Sanders, P.R., Krejany, E., Nie, C.Q., Fu, P., Bach, L.A., Wunderlich, G., Crabb, B.S., and Gilson, P.R. (2013). Inhibition of Plasmodium falciparum CDPK1 by conditional expression of its J-domain demonstrates a key role in schizont development. Biochem J *452*, 433-441.
22. Kim, D.I., and Roux, K.J. (2016). Filling the Void: Proximity-Based Labeling of Proteins in Living Cells. Trends Cell Biol *26*, 804-817.
23. Roux, K.J., Kim, D.I., Raida, M., and Burke, B. (2012). A promiscuous biotin ligase fusion protein identifies proximal and interacting proteins in mammalian cells. J Cell Biol *196*, 801-810.
24. Qin, W., Cho, K.F., Cavanagh, P.E., and Ting, A.Y. (2021). Deciphering molecular interactions by proximity labeling. Nat Methods *18*, 133-143.
25. Geiger, M., Brown, C., Wichers, J.S., Strauss, J., Lill, A., Thuenauer, R., Liffner, B., Wilcke, L., Lemcke, S., Heincke, D., et al. (2020). Structural Insights Into PfARO and Characterization of

its Interaction With PfAIP. J Mol Biol *432*, 878-896.

26. Boucher, M.J., Ghosh, S., Zhang, L., Lal, A., Jang, S.W., Ju, A., Zhang, S., Wang, X., Ralph, S.A., Zou, J., et al. (2018). Integrative proteomics and bioinformatic prediction enable a high-confidence apicoplast proteome in malaria parasites. PLoS Biol *16*, e2005895.

27. Schnider, C.B., Bausch-Fluck, D., Bruhlmann, F., Heussler, V.T., and Burda, P.C. (2018). BioID Reveals Novel Proteins of the Plasmodium Parasitophorous Vacuole Membrane. mSphere *3*.

28. Khosh-Naucke, M., Becker, J., Mesen-Ramirez, P., Kiani, P., Birnbaum, J., Frohlke, U., Jonscher, E., Schluter, H., and Spielmann, T. (2018). Identification of novel parasitophorous vacuole proteins in P. falciparum parasites using BioID. Int J Med Microbiol *308*, 13-24.

29. Kehrer, J., Frischknecht, F., and Mair, G.R. (2016). Proteomic Analysis of the Plasmodium berghei Gametocyte Egressome and Vesicular bioID of Osmiophilic Body Proteins Identifies Merozoite TRAP-like Protein (MTRAP) as an Essential Factor for Parasite Transmission. Mol Cell Proteomics *15*, 2852-2862.

30. Wichers, J.S., Wunderlich, J., Heincke, D., Pazicky, S., Strauss, J., Schmitt, M., Kimmel, J., Wilcke, L., Scharf, S., von Thien, H., et al. (2021). Identification of novel inner membrane complex and apical annuli proteins of the malaria parasite Plasmodium falciparum. Cell Microbiol, e13341.

31. May, D.G., Scott, K.L., Campos, A.R., and Roux, K.J. (2020). Comparative Application of BioID and TurboID for Protein-Proximity Biotinylation. Cells *9*.

32. Bosch, J.A., Chen, C.L., and Perrimon, N. (2021). Proximity-dependent labeling methods for proteomic profiling in living cells: An update. Wiley Interdiscip Rev Dev Biol *10*, e392.

33. Branon, T.C., Bosch, J.A., Sanchez, A.D., Udeshi, N.D., Svinkina, T., Carr, S.A., Feldman, J.L., Perrimon, N., and Ting, A.Y. (2018). Efficient proximity labeling in living cells and organisms with TurboID. Nat Biotechnol *36*, 880-887.

34. Otto, T.D., Bohme, U., Jackson, A.P., Hunt, M., Franke-Fayard, B., Hoeijmakers, W.A., Religa, A.A., Robertson, L., Sanders, M., Ogun, S.A., et al. (2014). A comprehensive evaluation of rodent malaria parasite genomes and gene expression. BMC Biol *12*, 86.

35. Wetzel, J., Herrmann, S., Swapna, L.S., Prusty, D., John Peter, A.T., Kono, M., Saini, S., Nellimarla, S., Wong, T.W., Wilcke, L., et al. (2015). The role of palmitoylation for protein recruitment to the inner membrane complex of the malaria parasite. J Biol Chem *290*, 1712-1728.

36. Li, Y., Zhong, C.Q., Xu, X., Cai, S., Wu, X., Zhang, Y., Chen, J., Shi, J., Lin, S., and Han, J. (2015). Group-DIA: analyzing multiple data-independent acquisition mass spectrometry data files. Nat Methods *12*, 1105-1106.

37. Gillet, L.C., Navarro, P., Tate, S., Rost, H., Selevsek, N., Reiter, L., Bonner, R., and Aebersold, R. (2012). Targeted data extraction of the MS/MS spectra generated by data-independent acquisition: a new concept for consistent and accurate proteome analysis. Mol Cell Proteomics *11*, O111 016717.

38. Hu, G., Cabrera, A., Kono, M., Mok, S., Chaal, B.K., Haase, S., Engelberg, K., Cheemadan, S., Spielmann, T., Preiser, P.R., et al. (2010). Transcriptional profiling of growth perturbations of the human malaria parasite Plasmodium falciparum. Nat Biotechnol *28*, 91-98.

39. Hodson, N., Invergo, B., Rayner, J.C., and Choudhary, J.S. (2015). Palmitoylation and palmitoyl-transferases in Plasmodium parasites. Biochemical Society transactions *43*, 240-245.

40. Parkyn Schneider, M., Liu, B., Glock, P., Suttie, A., McHugh, E., Andrew, D., Batinovic, S.,

Williamson, N., Hanssen, E., McMillan, P., et al. (2017). Disrupting assembly of the inner membrane complex blocks Plasmodium falciparum sexual stage development. PLoS Pathog *13*, e1006659.

41. Yeoman, J.A., Hanssen, E., Maier, A.G., Klonis, N., Maco, B., Baum, J., Turnbull, L., Whitchurch, C.B., Dixon, M.W., and Tilley, L. (2011). Tracking Glideosome-associated protein 50 reveals the development and organization of the inner membrane complex of Plasmodium falciparum. Eukaryot Cell *10*, 556-564.
42. Vaid, A., Thomas, D.C., and Sharma, P. (2008). Role of Ca2+/calmodulin-PfPKB signaling pathway in erythrocyte invasion by Plasmodium falciparum. J Biol Chem *283*, 5589-5597.
43. Dearnley, M.K., Yeoman, J.A., Hanssen, E., Kenny, S., Turnbull, L., Whitchurch, C.B., Tilley, L., and Dixon, M.W. (2012). Origin, composition, organization and function of the inner membrane complex of Plasmodium falciparum gametocytes. J Cell Sci *125*, 2053-2063.
44. Szklarczyk, D., Gable, A.L., Lyon, D., Junge, A., Wyder, S., Huerta-Cepas, J., Simonovic, M., Doncheva, N.T., Morris, J.H., Bork, P., et al. (2019). STRING v11: protein-protein association networks with increased coverage, supporting functional discovery in genome-wide experimental datasets. Nucleic Acids Res *47*, D607-D613.
45. Pieperhoff, M.S., Schmitt, M., Ferguson, D.J., and Meissner, M. (2013). The role of clathrin in post-Golgi trafficking in Toxoplasma gondii. PLoS One *8*, e77620.
46. Gordon, J.L., Beatty, W.L., and Sibley, L.D. (2008). A novel actin-related protein is associated with daughter cell formation in Toxoplasma gondii. Eukaryot Cell *7*, 1500-1512.
47. Bannister, L.H., Hopkins, J.M., Fowler, R.E., Krishna, S., and Mitchell, G.H. (2000). Ultrastructure of rhoptry development in Plasmodium falciparum erythrocytic schizonts. Parasitology *121 (Pt 3)*, 273-287.
48. Fang, H., Gomes, A.R., Klages, N., Pino, P., Maco, B., Walker, E.M., Zenonos, Z.A., Angrisano, F., Baum, J., Doerig, C., et al. (2018). Epistasis studies reveal redundancy among calcium-dependent protein kinases in motility and invasion of malaria parasites. Nat Commun *9*, 4248.
49. Wilde, M.L., Triglia, T., Marapana, D., Thompson, J.K., Kouzmitchev, A.A., Bullen, H.E., Gilson, P.R., Cowman, A.F., and Tonkin, C.J. (2019). Protein Kinase A Is Essential for Invasion of Plasmodium falciparum into Human Erythrocytes. mBio *10*.
50. Patil, H., Hughes, K.R., Lemgruber, L., Philip, N., Dickens, N., Starnes, G.L., and Waters, A.P. (2020). Zygote morphogenesis but not the establishment of cell polarity in Plasmodium berghei is controlled by the small GTPase, RAB11A. PLoS Pathog *16*, e1008091.
51. Green, J.L., Martin, S.R., Fielden, J., Ksagoni, A., Grainger, M., Yim Lim, B.Y., Molloy, J.E., and Holder, A.A. (2006). The MTIP-myosin A complex in blood stage malaria parasites. J Mol Biol *355*, 933-941.
52. Fukata, Y., and Fukata, M. (2010). Protein palmitoylation in neuronal development and synaptic plasticity. Nat Rev Neurosci *11*, 161-175.
53. Jones, M.L., Collins, M.O., Goulding, D., Choudhary, J.S., and Rayner, J.C. (2012). Analysis of protein palmitoylation reveals a pervasive role in Plasmodium development and pathogenesis. Cell Host Microbe *12*, 246-258.
54. Forrester, M.T., Hess, D.T., Thompson, J.W., Hultman, R., Moseley, M.A., Stamler, J.S., and Casey, P.J. (2011). Site-specific analysis of protein S-acylation by resin-assisted capture. J Lipid Res *52*, 393-398.
55. Santos, J.M., Kehrer, J., Franke-Fayard, B., Frischknecht, F., Janse, C.J., and Mair, G.R. (2015).

The Plasmodium palmitoyl-S-acyl-transferase DHHC2 is essential for ookinete morphogenesis and malaria transmission. Sci Rep *5*, 16034.

56. Liu, C., Yang, Z., Cai, M., Shi, Y., Cui, H., and Yuan, J. (2020). Generation of Plasmodium yoelii malaria parasite for conditional degradation of proteins. Mol Biochem Parasitol, 111346.
57. Janse, C.J., Ramesar, J., and Waters, A.P. (2006). High-efficiency transfection and drug selection of genetically transformed blood stages of the rodent malaria parasite Plasmodium berghei. Nat Protoc *1*, 346-356.
58. Blackman, M.J., Scott-Finnigan, T.J., Shai, S., and Holder, A.A. (1994). Antibodies inhibit the protease-mediated processing of a malaria merozoite surface protein. J Exp Med *180*, 389-393.
59. Child, M.A., Epp, C., Bujard, H., and Blackman, M.J. (2010). Regulated maturation of malaria merozoite surface protein-1 is essential for parasite growth. Mol Microbiol *78*, 187-202.
60. Silmon de Monerri, N.C., Flynn, H.R., Campos, M.G., Hackett, F., Koussis, K., Withers-Martinez, C., Skehel, J.M., and Blackman, M.J. (2011). Global identification of multiple substrates for Plasmodium falciparum SUB1, an essential malarial processing protease. Infect Immun *79*, 1086-1097.
61. Tao, N., Wagner, S.J., and Lublin, D.M. (1996). CD36 is palmitoylated on both N- and C-terminal cytoplasmic tails. J Biol Chem *271*, 22315-22320.
62. Sanchez, A.D., Branon, T.C., Cote, L.E., Papagiannakis, A., Liang, X., Pickett, M.A., Shen, K., Jacobs-Wagner, C., Ting, A.Y., and Feldman, J.L. (2021). Proximity labeling reveals non-centrosomal microtubule-organizing center components required for microtubule growth and localization. Curr Biol *31*, 3586-3600 e3511.
63. Bijlmakers, M.J., and Marsh, M. (2003). The on-off story of protein palmitoylation. Trends Cell Biol *13*, 32-42.
64. Foe, I.T., Child, M.A., Majmudar, J.D., Krishnamurthy, S., van der Linden, W.A., Ward, G.E., Martin, B.R., and Bogyo, M. (2015). Global Analysis of Palmitoylated Proteins in Toxoplasma gondii. Cell Host Microbe *18*, 501-511.
65. Hopp, C.S., Balaban, A.E., Bushell, E.S., Billker, O., Rayner, J.C., and Sinnis, P. (2016). Palmitoyl transferases have critical roles in the development of mosquito and liver stages of Plasmodium. Cell Microbiol *18*, 1625-1641.
66. Santos, J.M., Duarte, N., Kehrer, J., Ramesar, J., Avramut, M.C., Koster, A.J., Dessens, J.T., Frischknecht, F., Chevalley-Maurel, S., Janse, C.J., et al. (2016). Maternally supplied S-acyl-transferase is required for crystalloid organelle formation and transmission of the malaria parasite. Proc Natl Acad Sci U S A *113*, 7183-7188.
67. Tay, C.L., Jones, M.L., Hodson, N., Theron, M., Choudhary, J.S., and Rayner, J.C. (2016). Study of Plasmodium falciparum DHHC palmitoyl transferases identifies a role for PfDHHC9 in gametocytogenesis. Cell Microbiol *18*, 1596-1610.
68. Green, J.L., Rees-Channer, R.R., Howell, S.A., Martin, S.R., Knuepfer, E., Taylor, H.M., Grainger, M., and Holder, A.A. (2008). The motor complex of Plasmodium falciparum: phosphorylation by a calcium-dependent protein kinase. J Biol Chem *283*, 30980-30989.
69. Ridzuan, M.A., Moon, R.W., Knuepfer, E., Black, S., Holder, A.A., and Green, J.L. (2012). Subcellular location, phosphorylation and assembly into the motor complex of GAP45 during Plasmodium falciparum schizont development. PLoS One *7*, e33845.
70. Leung, J.M., He, Y., Zhang, F., Hwang, Y.C., Nagayasu, E., Liu, J., Murray, J.M., and Hu, K. (2017). Stability and function of a putative microtubule-organizing center in the human parasite

Toxoplasma gondii. Mol Biol Cell *28*, 1361-1378.

71. Zhang, C., Xiao, B., Jiang, Y., Zhao, Y., Li, Z., Gao, H., Ling, Y., Wei, J., Li, S., Lu, M., et al. (2014). Efficient editing of malaria parasite genome using the CRISPR/Cas9 system. MBio *5*, e01414-01414.

72. Magi, B., and Liberatori, S. (2005). Immunoblotting techniques. Methods Mol Biol *295*, 227-254.

73. da Veiga Leprevost, F., Haynes, S.E., Avtonomov, D.M., Chang, H.Y., Shanmugam, A.K., Mellacheruvu, D., Kong, A.T., and Nesvizhskii, A.I. (2020). Philosopher: a versatile toolkit for shotgun proteomics data analysis. Nat Methods *17*, 869-870.

74. Wang, D., Gan, G., Chen, X., and Zhong, C.Q. (2021). QuantPipe: A User-Friendly Pipeline Software Tool for DIA Data Analysis Based on the OpenSWATH-PyProphet-TRIC Workflow. J Proteome Res *20*, 1096-1102.

75. Rosenberger, G., Bludau, I., Schmitt, U., Heusel, M., Hunter, C.L., Liu, Y., MacCoss, M.J., MacLean, B.X., Nesvizhskii, A.I., Pedrioli, P.G.A., et al. (2017). Statistical control of peptide and protein error rates in large-scale targeted data-independent acquisition analyses. Nat Methods *14*, 921-927.

76. Tyanova, S., Temu, T., Sinitcyn, P., Carlson, A., Hein, M.Y., Geiger, T., Mann, M., and Cox, J. (2016). The Perseus computational platform for comprehensive analysis of (prote)omics data. Nat Methods *13*, 731-740.

77. Tupper, J., Stratford, M.R., Hill, S., Tozer, G.M., and Dachs, G.U. (2010). In vivo characterization of horseradish peroxidase with indole-3-acetic acid and 5-bromoindole-3-acetic acid for gene therapy of cancer. Cancer Gene Ther *17*, 420-428.

78. Aurrecoechea, C., Brestelli, J., Brunk, B.P., Dommer, J., Fischer, S., Gajria, B., Gao, X., Gingle, A., Grant, G., Harb, O.S., et al. (2009). PlasmoDB: a functional genomic database for malaria parasites. Nucleic Acids Res *37*, D539-543.

79. Aurrecoechea, C., Barreto, A., Basenko, E.Y., Brestelli, J., Brunk, B.P., Cade, S., Crouch, K., Doherty, R., Falke, D., Fischer, S., et al. (2017). EuPathDB: the eukaryotic pathogen genomics database resource. Nucleic Acids Res *45*, D581-D591.

80. Stecher, G., Liu, L., Sanderford, M., Peterson, D., Tamura, K., and Kumar, S. (2014). MEGA-MD: molecular evolutionary genetics analysis software with mutational diagnosis of amino acid variation. Bioinformatics *30*, 1305-1307.

81. Ren, J., Wen, L., Gao, X., Jin, C., Xue, Y., and Yao, X. (2008). CSS-Palm 2.0: an updated software for palmitoylation sites prediction. Protein Eng Des Sel *21*, 639-644.

82. von Mering, C., Huynen, M., Jaeggi, D., Schmidt, S., Bork, P., and Snel, B. (2003). STRING: a database of predicted functional associations between proteins. Nucleic Acids Res *31*, 258-261.

Materials and Methods

Animal usage and ethics statement

All animal experiments were performed by approved protocols (XMULAC20140004) by the Committee for Care and Use of Laboratory Animals of Xiamen University. The ICR mice (female, 5 to 6 weeks old) were purchased from the Animal Care Center of

Xiamen University and used for parasite propagation, drug selection, and parasite cloning.

Plasmid construction and parasite transfection

CRISPR/Cas9 plasmid pYCm was used for parasite genomic modification [70, 71]. To construct the plasmids for gene deletion, the N- or C-terminal segments (400–600 bp) of the coding regions were PCR-amplified as the left or right homologous arm or 400–600 bp from 5-UTR or 3-UTR following the translation stop codon as left or right arm, respectively. To construct the plasmids for gene tagging, the DNA fragment (encoding 6HA, 4Myc, GFP, or mAID-2HA) was inserted between the left and right arms in frame with the gene of interest. For each gene tagging, two sgRNAs were designed to target sites close to the N- or C-terminal part of the coding region. To construct the plasmid for amino acid substitution, the donor template (700-800 bp) for homologous recombination was introduced with the targeted mutations for amino acid substitution and extra shield mutations via mutagenesis. These shield mutations in or adjacent to the protospacer-adjacent motif (PAM) were used to prevent the recognition and cleavage of the replaced locus by the gRNA/Cas9 complex. Seven sgRNAs were designed to target sites close to the desired mutation sites. The PCR primers and DNA oligonucleotides used are listed in the Table S2. Blood with 15–25% parasitemia was collected from infected mice and cultured in RPMI-1640 (Gibco, cat#11879020) supplied with 20% FBS (Gibco, cat#10099) at 37°C for 3 h for schizont development. After washing two times with RPMI-1640, the parasite were electroporated with 5-10 μg purified circular plasmid DNA using Lonza Nucleotector. Transfected parasites were immediately intravenously injected into a naïve mouse and applied to pyrimethamine pressure (provided in drinking water at concentration 7 mg/ml) from 24 h post transfection. Parasites with transfected plasmids usually appear about 5 to 7 days after drug selection. Genomic DNA of parasites were extracted for genotyping PCR analysis. Parasite clones with correct modification were obtained using the limiting dilution method.

948 **Genotypic analysis of transgenic parasites**

949 All transgenic parasites were generated from the *P. yoelii* 17XNL or *Tir1* strains.
950 Infected blood samples from transfected mice were collected from the tail of mice and
951 lysed by 1% saponin in PBS. Parasite genomic DNAs were extracted using DNeasy
952 Blood Kits (Qiagen). For each genetic modification, both 5' and 3' homologous
953 recombination were detected by PCR to confirm successful integration of homologous
954 arms. The PCR primers used for genotyping are listed in the Table S2. Positive clones
955 with correct modifications were obtained after limiting dilution. The PCR-genotyping
956 results confirming the genetic modified parasites were shown in the Fig S9.

957

958 **Parasite negative selection with 5-Fluorouracil**

959 Modified parasites subjected for sequential modification were negatively selected to
960 remove pYCm plasmid. 5-fluorouracil (5-FC, Sigma-Aldrich, cat#F6627) was
961 prepared in drinking water at a final concentration of 2.0 mg/ml. A naïve mouse
962 receiving parasites with residual plasmid was subjected to 5-FC selection for 6-8 days.
963 Diagnostic PCR was performed to confirm the complete removal of plasmid in the
964 parasites. The PCR primers used are listed in the Table S2.

965

966 **DNA mutagenesis for amino acid replacement**

967 For the amino acid replacement in the proteins of interest, the wildtype gene cDNAs
968 were cloned into NheI and NcoI sites in the pL0019-HA/Myc vector (*isp3* gene
969 promoter for parasite asexual blood stages) or pcDNA3.1-HA/Myc vector (CMV
970 promoter for mammalian cell). A PCR-based protocol with mutagenic oligonucleotides
971 was used to generate the gene mutants. The primers used are listed in the Table S2.

972

973 **Protein transient expression in asexual blood stage parasites**

974 For protein transient expression, the coding sequence of target genes was tagged N-or
975 C-terminally with an epitope tag and driven by the regulatory regions of the *isp3* gene
976 (1.5 kb of the 5'-UTR and 1 kb of the 3'-UTR). Gene expression cassettes were inserted
977 into the pL0019-derived vector containing a human *dhfr* marker for pyrimethamine

978 selection. Blood stage parasites were electroporated with 10 μg vector plasmid DNA
979 and selected with pyrimethamine (70 μg/ml) for 7 days. Parasites appearing after
980 pyrimethamine selection were used for further experiments.
981
982 **Antibodies and antiserum**
983 The primary antibodies used included: rabbit anti-HA (Western blot, 1:1000, IFA,
984 1:1000, 3724S, Cell Signaling Technology (CST)), mouse anti-HA (IFA, 1:500, sc-
985 57592, Santa Cruz Biotechnology), rabbit anti-Myc (Western blot, 1:1000, 2276S,
986 CST), mouse anti-Myc (IFA, 1:500, sc-40, Santa Cruz Biotechnology) and rabbit anti-
987 Histone H3 (western blot, 1:2000, 9715, CST). The secondary antibodies used included:
988 goat anti-rabbit IgG HRP-conjugated and goat anti-mouse IgG HRP-conjugated
989 secondary antibody (1:5000, Abcam), Alexa Fluor 555 goat anti-rabbit IgG (1:1000,
990 Thermo Fisher Scientific), Alexa Fluor 488 goat anti-rabbit IgG (1:1000, Thermo
991 Fisher Scientific), Alexa Fluor 555 goat anti-mouse IgG (1:1000, Thermo Fisher
992 Scientific), Alexa Fluor 488 goat anti-mouse IgG (1:1000, Thermo Fisher Scientific),
993 and Alexa Fluor 488 conjugated streptavidin (1:1000, Invitrogen, S32354). Antiserums,
994 including rabbit anti-GAP45 (Western blot, 1:1000, IFA, 1:1000), mouse anti-GAP45
995 (IFA, 1:1000), and rabbit anti-BiP (Western blot, 1:1000) were described in previous
996 studies [17]. Other antiserums, including rabbit anti-CDPK1 (Western blot, 1:1000, IFA,
997 1:500), rabbit anti-Erd2 (Western blot, 1:1000), and rabbit anti-MSP1 (Western blot,
998 1:2000, IFA, 1:1000) were prepared by immunization of rabbit or mouse with
999 recombinant protein as antigens: for CDPK1 (D_{11}VRGNK…CDNKPF$_{523}$), for Erd2
1000 (E_{38}LYLIV…PFNGEV$_{221}$), and for MSP1 (V_{1413}YTKRL…GVFCSS$_{1752}$).
1001
1002 **Immunofluorescence assays**
1003 Cells were fixed with 4% paraformaldehyde for 15 min and rinsed with PBS three
1004 times. The cells were then permeabilized with 0.1% Triton X-100 for 10 min, rinsed
1005 with PBS twice, and incubated with 5% BSA for 1 h. They were incubated with the
1006 primary antibodies overnight at 4°C, rinsed with PBS three times, and incubated with
1007 fluorescent conjugated secondary antibodies for 1 h in the dark. After washing with

PBS, the cells were stained with DNA dye Hoechst 33342 for 10 min and mounted on glass slides using the mounting medium. Images were captured using identical settings under Zeiss LSM 880 confocal microscope.

Live cell imaging

Parasites expressing GFP-fused proteins were collected in 200 µL PBS, washed twice with PBS and stained with Hoechst 33342 at room temperature for 10 min. After centrifugation at 300 g for 5 min, the parasites pellets were re-suspended in 100 µL of 3% low melting agarose, spread evenly on the bottom of 35 mm plate, and followed by cooling at RT for 15 min. The parasites were imaged by a Zeiss 880 confocal microscope with the 63×/1.40 oil objective.

Airyscan super-resolution microscopy

Parasites were imaged using a 100×/1.46 NA oil immersion objective on a Zeiss LSM880 fitted with an Airyscan detector. Super-resolution reconstructions of multi-labelled *dhhc2::6HA* schizonts were acquired, sequentially in three channels, as follows: channel 1= 561 nm laser (HA), channel 2 = 488 nm laser (GAP45), channel 3 = 405 nm laser (Hoechst 33342). Images were acquired using a defined region of interest (ROI) with an average of two, with 2,048 × 2,048 pixels of image size and 8-bit image depth. Every part of each image remains fully within the dynamic range of pixel intensity. Three-dimensional (3D) Z-stacks were acquired at 0.25 µm intervals in Z axis using piezo drive prior to being Airyscan processed in 3D using batch mode in ZEN Black (Zeiss). Maximum intensity projections of super-resolution images were output with the default setting.

Protein extraction and immunoblot

Parasite total proteins from asexual blood stages were extracted with RIPA Lysis Buffer (50 mM pH 7.4 Tris, 150 mM NaCl, 1% Triton X-100, 1% sodium deoxycholate, 0.1% SDS, 1 mM EDTA) containing protease inhibitor cocktail and PMSF. After ultra-sonication, the lysates were incubated on ice for 30 min before centrifugation at 12, 000

g for 10 min at 4°C. The supernatant was then lysed in Laemmli sample buffer, stored at 4°C for immunoblot. Protein samples were separated in SDS-PAGE, transferred to PVDF membrane that was blocked by 5% skim milk in TBST, and then incubated with primary antibodies. After incubation, the membrane was washed three times with TBST and incubated with HRP-conjugated secondary antibodies. The membrane was washed four times in TBST before the enhanced chemiluminescence detection.

Dot blot detecting biotinylated proteins

Dot blot assay of the biotinylated proteins was performed as described previously [72]. Freshly extracted proteins were quantified using the Pierce BCA Protein Assay kit (Thermo Scientific, cat#23227). PVDF membrane pre-activated by methanol was prepared. Equal amounts of total proteins (~2 μg) from each sample were loaded onto the PVDF membrane surface. After protein absorbing and air-dry, the PVDF membrane was blocked by 5% skim milk in TBST and incubated with HRP-conjugated streptavidin (GenScript, M00091) for the enhanced chemiluminescence detection. MSP1 protein was used as the loading control.

Protein solubility assay

Purified schizonts (1×10^6) from each sample were used for protein solubility assay. Parasites were lysed in 100 μl of hypotonic buffer (10 mM Hepes, 10 mM KCl, pH 7.4) and frozen and thawed (-80°C to 37°C) twice for cell lysis. The lysates were centrifuged at 12,000 g for 5 min at 4°C, and the supernatants containing cytosolic soluble proteins were collected as "Hypo" fraction. The pellet was then rinsed with 1 ml of ice-cold PBS, re-suspended in 100 μl of freshly prepared carbonate buffer (0.1 M Na_2CO_3), kept on ice for 30 min, and then centrifuged at 12,000 g for 5 min at 4°C. The supernatants containing peripheral membrane proteins were collected as "Carb" fraction. The pellet was rinsed with 1 ml of ice-cold PBS, re-suspended in 100 μl of freshly prepared Triton X-100 buffer (1% Triton X-100), kept on ice for another 30 min, and centrifuged at 12,000 g for 5 min at 4°C. The supernatants containing integral membrane proteins were collected as "Trx" fraction. The final pellet including insoluble proteins and non-

protein materials was solubilized in 1× Laemmli sample buffer as "pellet" fraction. All fractions were boiled at 95°C for 10 min and centrifuged at 12,000 g for 5 min. Equal volume of supernatants from each sample was used for immunoblot. For detecting the change in IMC localization of palmitoylated proteins, Hypo fractions were referred to "light fraction", while Hypo-insoluble fractions were referred to "heavy fraction". All buffers used in this assay contain the protease inhibitor cocktail (MedChemExpress, cat#HY-K0010).

Purification of schizont and ring/trophozoite stage parasites

The asexual blood stage parasites with 15-25% parasitemia were cultured in RPMI-1640 medium supplied with 20% fetal bovine serum (FBS) and 100 IU penicillin, 100 mg/ml streptomycin at 37°C for 3 h for increasing schizont production. The schizonts were purified using the Nycodenz density gradient centrifugation. Briefly, the schizonts were suspended in RPMI-1640 and 7 ml of the schizont culture was loaded on the top of a 2 ml of the 60% Nycodenz solution in a 15 ml centrifugation tube. After centrifugation at 300g for 30 min and removing the supernatants, top layer containing the schizonts were collected. Rings and early trophozoites were collected at the bottom with uninfected erythrocytes.

TurboID-based proximity-labelling and Pull-down

The schizonts expressing the biotin ligase TurboID or BioID were purified using the methods described above. After incubating with 100 μM biotin (Sigma-Aldrich, cat#B4639) at 37°C for 3 h, the schizonts were lysed with 0.01% saponin and stored at -80°C. For pull-down, parasites were lysed in RIPA buffer (50 mM Tris-HCl pH 7.4, 150 mM NaCl, 1% NP40, 0.1% SDS, 1% Sodium deoxycholate, 1% TritonX-100, 1 mM EDTA) containing protease inhibitor cocktail and PMSF. 10 mg of cell lysates were collected as a biological replicate and incubated with 100 μL of streptavidin sepharose (Thermal Scientific, cat#SA10004). After incubation overnight at 4°C, streptavidin beads were then washed with the following procedures: twice with RIPA lysis buffer, once with 2 M urea in 10 mM Tris-HCl, pH 8.0, and two more times with

50 mM Tris-HCl (pH 8.5). The washed beads were re-suspended in 200 µL 50 mM Tris-HCl (pH 8.5). The biotinylated proteins were digested on-bead by rolling with 1 µg of trypsin for 16 h at 37°C followed by a second digest with 0.5 µg trypsin for 2 hours.

Protein digestion and peptide desalting

The enriched biotinylated proteins were digested on-bead by rolling with 1 µg of trypsin for 16 h at 37°C followed by a second digest with 0.5 µg trypsin for 2 hours. For digested peptide samples, StageTips packed with SDB-RPS (2241, 3 M) material (made in-house) was used for desalting. Brifely, about 1% trifluoroacetic acid (TFA; Sigma-Aldrich, cat#T6508) was added into the reactions to stop digestion. The SDB-RPS StageTips were conditioned with 100 µl 100% acetonitrile (ACN) (Sigma-Aldrich, cat#3485). The peptides were loaded into StageTips, followed by centrifugation at 4000 g for 5 min. StageTips were washed twice with 100 µl 1% TFA/ isopropyl alcohol (Sigma-Aldrich, cat#I9030), and then washed with 100 µl 0.2% TFA. Elution of peptides was performed using 80% ACN/5% ammonia water. All eluted materials were collected in glass vials (A3511040; CNW Technologies) and dried at 45°C using a SpeedVac centrifuge (Eppendorf Concentrator Plus; 5305).

Mass spectrometry

Digested peptides were dissolved in 0.1% formic acid (Sigma-Aldrich, cat#06440) containing independent retention time (iRT) peptides and analyzed by Sequential Window Acquisition of All Theoretical Mass Spectra (SWATH-MS) on TripleTOF 5600. For SWATH-MS, an MS1 scan records a 350 to 1250 m/z range for 250 ms, and a 100 to 1800 m/z range was recorded for 33.3 ms in the high-sensitivity mode MS2 scan. One MS1 scan was followed by 100 MS2 scans, which covered a precursor m/z range from 400 to 1200. SWATH-MS wiff files were converted to centroid mzXML files using MSConvert (version 3.0.19311), which were then subjected to DIA-Umpire software (version 2.1.6) for analysis. Signal-extraction module of DIA-Umpire was used to generate pseudo-DDA mgf files. These mgf files were converted to mzML files,

which are subjected to database search using MSFragger (version 2.3) through the FragPipe interface (https://fragpipe.nesvilab.org/). The search parameters were set as followed: precursor monoisotopic mass tolerance '50 ppm' fragment mass tolerance '0.1 Da', modification '57.021464@C', potential modification mass '15.994915@M', cleavage 'semi' and maximum missed cleavage sites '1'. PeptideProphet, ProteinProphet and FDR filtering were performed by Philosopher software (version 3.2.2) (https://github.com/Nesvilab/philosopher) through the FragPipe interface (https://fragpipe.nesvilab.org/) [73]. The pep.xml search results were validated and scored using PeptideProphet followed by analysis with ProteinProphet. The precursor ions and proteins were filtered at 1% FDR. The spectral library was generated by using EasyPQP tool (version 0.1.12) which is integrated in the FragPipe software. SWATH-MS files were converted to profile mzXML files. The spectral library based targeted analysis of SWATH-MS was performed using the QuantPipe tool based on the OpenSWATH-PyProphet-Tric workflow [74, 75]. The results were filtered at 1% global protein FDR. Statistical analysis by Perseus software (version 1.6.10.43) were performed as previously reported [76]. Parasite protein intensities were imported into Perseus. Protein abundances were normalized with total intensities of all proteins per run and then log2 transformed. The Pearson correlation analysis, hierarchical clustering, and volcano plots were performed with default settings.

Chemical treatment of parasite

To evaluate the effects of 2-BP on parasite protein palmitoylation and localization, 2-BP (Sigma-Aldrich, cat#21604) was added to parasite culture at a final concentration of 100 μM at 37℃ for the time indicated in each experiment. To deplete the target parasite proteins *in vitro* by auxin-induced protein degradation, the parasite culture was added with a final concentration of 1mM IAA (Sigma-Aldrich, cat#I2886) or vehicle (DMSO 1:1000) at 37℃ for 3-12 h with ambient ~5% CO_2 levels. To deplete the target parasite proteins in mice, mice were administered with either IAA or vehicle intraperitoneally. Each mouse was injected with 0.2 mL of PBS containing IAA (20

mg/mL IAA, 3 mM NaOH, pH 7.4) or vehicle (similar solution without IAA). The usage of this dosage of IAA in mice was referred to a previous study [77].

Quantitative real-time PCR

Purified parasites were prepared for extraction of total RNAs. Following isolation with TRIzol (Invitrogen), total RNA was purified with the RNAeasy Mini Kit (QIAGEN, cat#74106). cDNA was then obtained with the TransScript® Two-Step RT-PCR SuperMix (TransGen Biotech, cat#AT401-01) and checked afterwards for gDNA contaminations via RT-PCR. The Real-time quantitative PCR was performed using SYBR Green Supermix (Bio-Rad, cat#1708882) in the Bio-Rad iCycler iQ system (Bio-Rad, USA). The primers used are listed in the Table S2. All runs under the following conditions: 95°C for 20 s followed by 40 cycles of 95°C for 3 s; 60°C for 30 s. The samples were run in triplicate and normalized to *gapdh* using a ΔΔ cycle threshold-based algorithm, to provide arbitrary units representing relative expression levels. Graphpad 8 was used for statistical analysis.

Flow cytometry analysis

Parasite-infected erythrocytes were collected from mice via tail vein or *in vitro* culture, washed twice with PBS, and suspended in PBS with Hoechst 33342 (Thermo Fisher Scientific, cat#62249) for nuclei staining. The parasites were analyzed by flow cytometry in a BD LSR Fortessa flow cytometer. Parasite-infected erythrocytes were gated using the fluorescence signal of 405 nm (Hoechst 33342), while uninfected erythrocytes were used as a control. All data were processed by FlowJo software.

***In vitro* trophozoite to schizont development**

Purified rings and early trophozoites via Nycodenz centrifugation were incubated with vehicle or IAA and cultured for 12 h at 37°C at ambient CO_2 (~5%). Mature schizonts developed from the early trophozoites were counted by thin blood smears with Giemsa staining.

Erythrocyte invasion of merozoite

Different from an automatous rupture of mature schizonts of the *in vitro* cultured *P. falciparum*, the *P. yoelii* schizonts displayed an arrest in rupture after maturation in the *in vitro* condition. 1.0×10^8 purified schizonts were incubated with vehicle and IAA respectively at 37℃ for 3 h to deplete the DHHC2 protein. After this, the schizonts were mechanically disrupted by vibrating for 1 h. Under these conditions, merozoite release occurs in about 50% of mature schizonts with both vehicle and IAA treatment. Similar number of merozoites were injected intravenously into each mouse with 3-4 naïve mice in each group. Mouse blood was collected for blood smears at 20 min after injection and the parasitemia of ring-stage was quantified by Giemsa solution staining and flow cytometry.

Mammalian cell culture and transient transfection

HEK293T cells were maintained in Dulbecco's modified Eagle's medium (DMEM) supplemented with 10% fetal bovine serum (FBS), 100 IU penicillin, 100 mg/ml streptomycin at 37℃ in a humidified incubator containing 5% CO_2. TurboFect transfection reagent (Thermo Fisher Scientific, cat#R0532) was used for cell transfection. Total DNA for each plate was adjusted to the same amount by using a relevant empty vector. Transfected cells were harvested at 48 h after transfection for further analysis.

Detection of protein palmitoylation

Protein palmitoylation was detected using the Acyl-RAC assay described previously [17]. Schizonts were lysed in DHHC Buffer B (2.5% SDS, 1 mM EDTA, 100 mM HEPES, pH 7.5) containing protease inhibitor cocktail and PMSF and incubated on ice for 30 min. After centrifugation at 12,000 g for 10 min, supernatant was collected and treated with 0.1% methyl methanethiosulfonate (MMTS) at 42°C for 15 min. MMTS was removed by acetone precipitation followed by washing with 70% acetone three times. Protein samples were solubilized in DHHC Buffer C (1% SDS, 1 mM EDTA, 100 mM HEPES, pH 7.5) and were captured on thiopropyl sepharose 6B (GE

Healthcare, 17-0402-01) in the presence of 2 M hydroxylamine or 2 M NaCl (negative control) by agitating for 3 h at room temperature. Loading controls (Input) were collected before addition of thiopropyl sepharose 6B beads. After five times washing with urea DHHC Buffer (1% SDS, 1 mM EDTA, 100 mM HEPES, 8 M urea, pH 7.5), the captured proteins were eluted from thiopropyl sepharose 6B beads in 60 µl DHHC Buffer C supplemented with 50 mM DTT, and mixed with Laemmli sample buffer for further western blot analysis.

Transmission electron microscopy

For transmission electron microscope (TEM), purified parasites were pre-fixed with 2.5% glutaraldehyde in 0.1 M phosphate buffer at 4℃ overnight, rinsed three times with PBS, then fixed with 1% osmium acid for 2 h, and rinsed three times with PBS. Fixed samples were dehydrated with concentration gradient acetone. After embedding and slicing, thin sections were stained with uranyl acetate and lead citrate. All samples were imaged using the HT-7800 electron microscope.

Bioinformatic analysis and tools

The genomic DNA sequences of target genes were downloaded from PlasmoDB database [78]. The sgRNAs of a target gene were designed using EuPaGDT [79]. Amino acid sequence alignment was analyzed using MEGA5.0 [80]. The palmitoylation sites in protein were predicted using CSS-Palm 4.0 [81]. The relationship of protein-protein interaction was analyzed with STRING (https://string-db.org)[82]. Gene ontology analysis were performed on the PlasmoDB database [78].

Quantification and statistical analysis

For quantification of protein expression in western blot, protein band intensity was quantified using Fiji software from three independent experiments. The signals of target proteins were normalized with that of control proteins. For quantification of protein expression in IFA, confocal fluorescence microscopy images were acquired under identical parameters. Fluorescent signals were quantified using Fiji software. More than

30 cells were analysed in each group. Protein relative expression was calculated as the signal intensity compared to that of control group. Statistical analysis was performed using GraphPad Software 5.0 .Two-tailed Student's t-test or Whiney Mann test was used to compare differences between treated groups and their paired controls. n represents the number of parasite cells tested in each group, or experimental replication. The exact value of n was indicated within the figures. P value in each statistical analysis was also indicated within the figures.

Data availability

Mass spectrometry proteomics data have been deposited to the ProteomeXchange Consortium and can be accessed via the PRIDE partner repository. The website for MS data is https://www.iprox.cn/page/PSV023.html;?url=1630462125518RngX. All other relevant data in this study are available from the authors upon request.

Figure 1

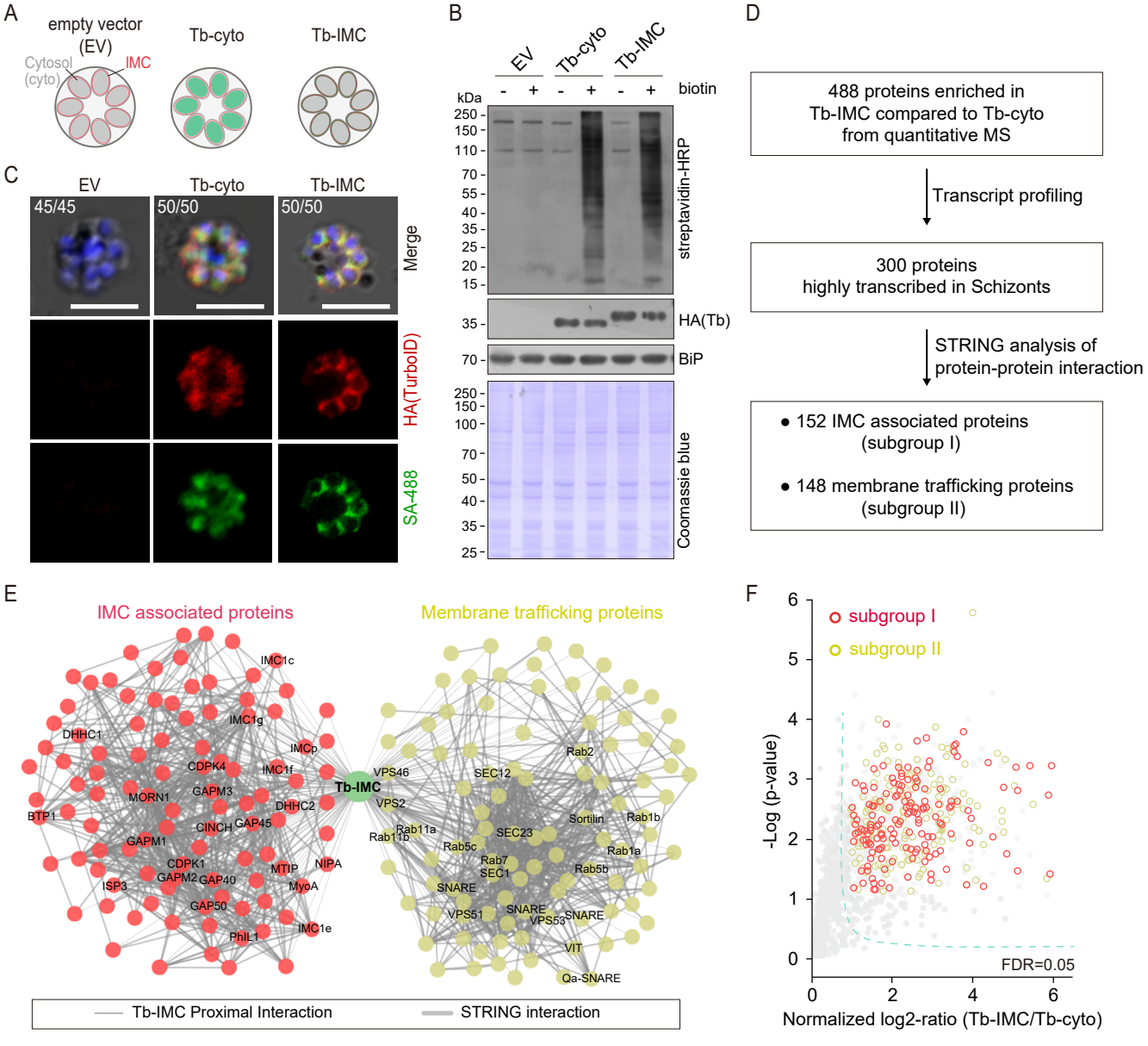
A
empty vector (EV)
Cytosol (cyto)
IMC
Tb-cyto
Tb-IMC
B
EV
Tb-cyto
Tb-IMC
kDa
- + - + - +
biotin
250
150
110
70
55
40
35
25
20
15
streptavidin-HRP
35
HA(Tb)
70
BiP
250
150
100
70
50
40
35
25
Coomassie blue
C
EV
Tb-cyto
Tb-IMC
45/45
50/50
50/50
Merge
HA(TurboID)
SA-488
D
488 proteins enriched in Tb-IMC compared to Tb-cyto from quantitative MS
Transcript profiling
300 proteins highly transcribed in Schizonts
STRING analysis of protein-protein interaction
• 152 IMC associated proteins (subgroup I)
• 148 membrane trafficking proteins (subgroup II)
E
IMC associated proteins
Membrane trafficking proteins
IMC1c
IMC1g
DHHC1
IMCp
CDPK4
IMC1f
MORN1
GAPM3
DHHC2
BTP1
CINCH
GAP45
GAPM1
CDPK1
MTIP
NIPA
ISP3
GAPM2
GAP40
MyoA
GAP50
PhIL1
IMC1e
Tb-IMC
VPS46
VPS2
Rab2
SEC12
Sortilin
Rab1b
Rab11b
Rab11a
SEC23
Rab5c
Rab1a
Rab7
SEC1
Rab5b
SNARE
VPS51
SNARE
VPS53
SNARE
VIT
Qa-SNARE
Tb-IMC Proximal Interaction
STRING interaction
F
subgroup I
subgroup II
-Log (p-value)
FDR=0.05
Normalized log2-ratio (Tb-IMC/Tb-cyto)

Figure 1. Proteomic of *P. yoelii* schizont IMC by TurboID and quantitative mass spectrometry

A. Schematic of schizonts with TurboID ligase localizing in cytoplasm (Tb-cyto) and IMC (Tb-IMC). EV indicates the schizonts expressing empty vector (EV). See the detailed information of Tb-IMC and Tb-cyto in the **Supplementary figure 2**.

B. Immunoblot and streptavidin blot of total lysate from the schizonts expressing the EV, Tb-cyto and Tb-IMC. Tagged ligase was detected by anti-HA antibody while biotinylated proteins were detected by streptavidin-conjugated horseradish peroxidase (streptavdin-HRP). Comparable loaded lysate was indicated by BiP control and Coomassie blue stain.

C. Co-staining of TurboID ligase and biotinylated proteins in the schizonts expressing the ligase of the EV, Tb-cyto, and Tb-IMC. The schizonts incubated with or without 100 μM biotin were co-stained with the SA-488 and anti-HA antibody. x/y in the figure is the number of cell displaying signal/the number of cells analyzed. Scale bar=5 μm.

D. Workflow for filtering the Tb-IMC interacting proteins (proximal interactors). 488 biotinylated proteins that were at least two times more abundant in Tb-IMC than that in Tb-cyto control at both three replicates and with an adjusted P value < 0.05, were significantly enriched. Detailed information in the **Supplementary figure 2**.

E. Interaction network of 300 Tb-IMC interacting proteins (STRING, p-value < 1.0e-16, bold lines). Two subgroups (I: left, II: right) were functionally clustered. Many known IMC or IMC-associated proteins were clustered into the subgroup I while many annotated ER/Golgi secretory or vesicle trafficking proteins were clustered into the subgroup II.

F. Volcano plots showing the 300 Tb-IMC interacting proteins. Relative biotinylation of each protein was calculated by quantifying protein intensity in Tb-IMC relative to Tb-cyto schizonts (n=3). Proteins in the subgroup I (red circle) and subgroup II (yellow circle) are indicated.

Figure 2

A

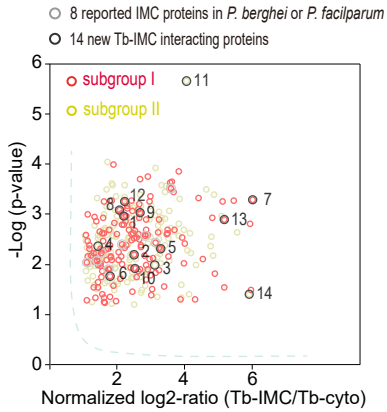

B

	gene ID	(annotation)	subgroup	IMC localization
1.	PY17X_0207400	(ATP synthase-associated protein)	○	no
2.	PY17X_0312400	(RING zinc finger protein)	○	yes
3.	PY17X_0417300	(YOP1)	○	no
4.	PY17X_0418000	(VPS46)	○	yes
5.	PY17X_0812700	(PMP1)	○	yes
6.	PY17X_0917100	(aquaglyceroporin)	○	no
7.	PY17X_1131200	(tetratricopeptide repeat protein)	○	yes
8.	PY17X_1139700	(Unknown function)	○	yes
9.	PY17X_1220300	(pPK 1)	○	yes
10.	PY17X_1348200	(Unknown function)	○	yes
11.	PY17X_1359500	(Rab11b)	○	yes
12.	PY17X_1411000	(RNA-binding protein)	○	yes
13.	PY17X_1441500	(Unknown function)	○	yes
14.	PY17X_1453100	(v-SNARE protein)	○	yes

C

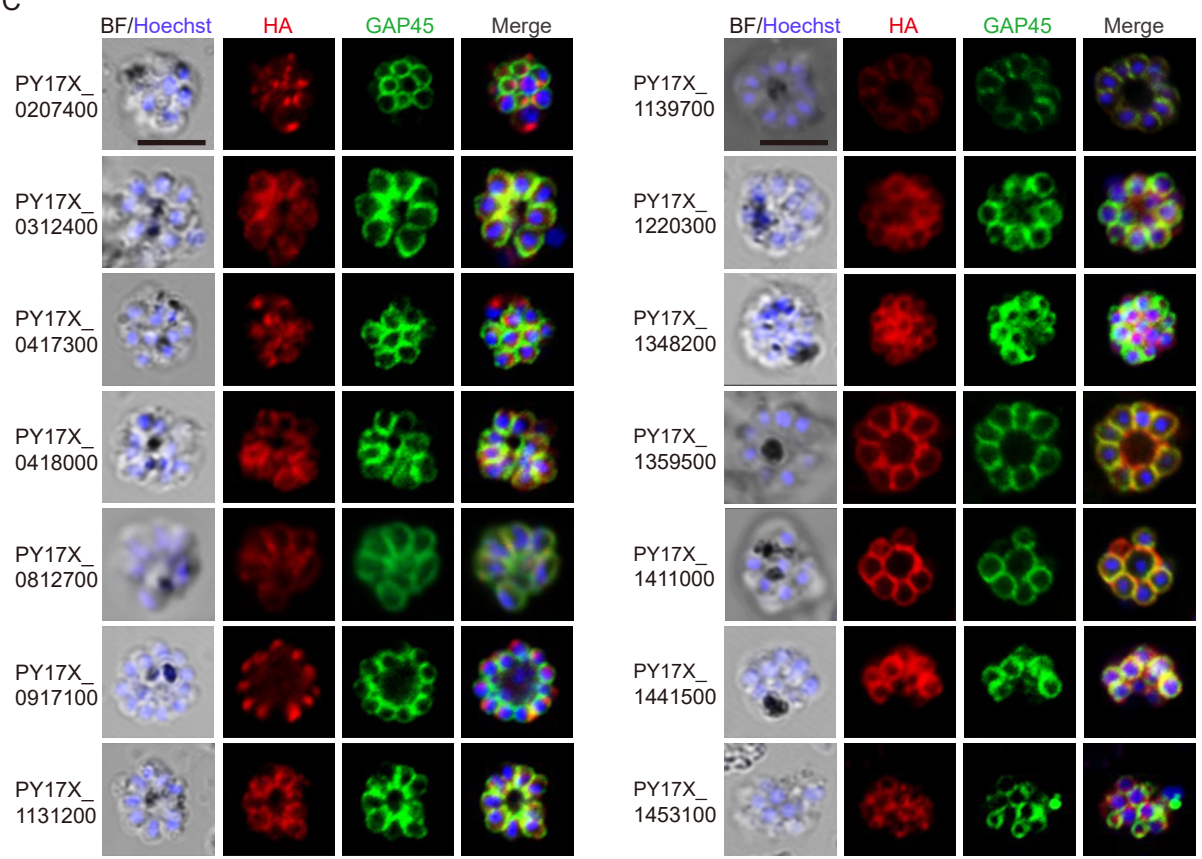

Figure 2. Validation of 11 new IMC proteins by localization analysis

A. 22 candidates selected from the Tb-IMC interacting proteins for subcellular localization analysis in the *P. yoelii*. The orthologues of 8 proteins (light gray dot) have been experimentally validated to be IMC-residing or -associated in the schizonts of *P. berghei* or *P. falciparum*, while subcellular localization of other 14 proteins (dark gray dot) have not been well-characterized in *Plasmodium* species.

B. Information and subcellular localization summary of the 14 newly tested Tb-IMC interacting proteins shown in **A**.

C. IFA analysis of 14 Tb-IMC interacting proteins in the *P. yoelii* schizonts. Each protein was tagged with a 6HA at the N- or C-terminus and episomally expressed in the schizonts. The schizonts were co-stained with antibodies against GAP45 and HA. Nuclei were stained with Hoechst 33342. Scale bar=5 μm.

Figure 3

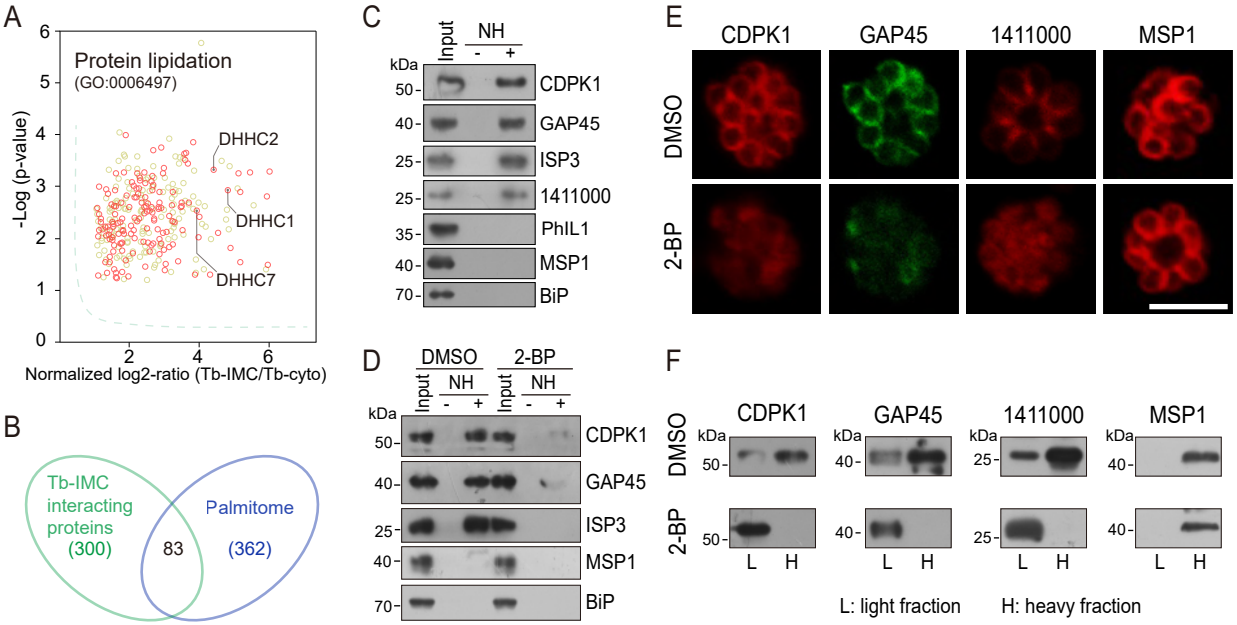
A
Protein lipidation
(GO:0006497)
DHHC2
DHHC1
DHHC7
-Log (p-value)
Normalized log2-ratio (Tb-IMC/Tb-cyto)
B
Tb-IMC interacting proteins (300)
83
Palmitome (362)
C
Input
NH
kDa
CDPK1
GAP45
ISP3
1411000
PhIL1
MSP1
BiP
D
DMSO
2-BP
Input
NH
E
CDPK1
GAP45
1411000
MSP1
DMSO
2-BP
F
L
H
L: light fraction
H: heavy fraction

Figure 3. Palmitoylation of certain IMC proteins and palmitoylation regulates protein localization

A. Enrichment of enzymes for protein lipidation in the Tb-IMC interacting proteins shown in the **Figure 1F**, including three palmitoyl-S-acyl-transferases DHHC2, DHHC1, and DHHC7.

B. Venn diagram showing overlap between Tb-IMC interactors (green) identified in this study and the orthologs within the *P. falciparum* palmitome (blue). 83 Tb-IMC interactors (overlap, 28%) were considered to be potentially palmitoylated. Numbers indicate the number of proteins identified.

C. Acyl-RAC method detecting palmitoylation of CDPK1, GAP45, ISP3, and PY17X_1411000, but not PhIL1 in schizonts. NH: NH_2OH. MSP1 and BiP served as loading controls. Total proteins were treated with MMTs to block the thiol side chain in free cysteine. Proteins with palmitoylated cysteine were re-exposed the thiol side chain with removal of palmitic acid by NH_2OH, purified via Thiopropyl Sepharose, and eluted by DTT for immunoblot. Two replicates performed.

D. Palmitoylation analysis of CDPK1, GAP45, and ISP3 in schizonts treated with 2-BP. NH: NH_2OH. MSP1 and BiP served as loading controls. Two replicates performed.

E. IFA analysis of CDPK1, GAP45, PY17X_1411000, and MSP1 in schizonts treated with 2-BP and DMSO respectively. Scale bar= 5 μm.

F. Fractionation analysis of CDPK1, GAP45, PY17X_1411000, and MSP1 in schizonts treated with 2-BP and DMSO respectively. Light fraction includes cytosolic proteins while heavy fraction includes membrane proteins and cytoskeleton proteins. Two replicates performed.

Figure 4

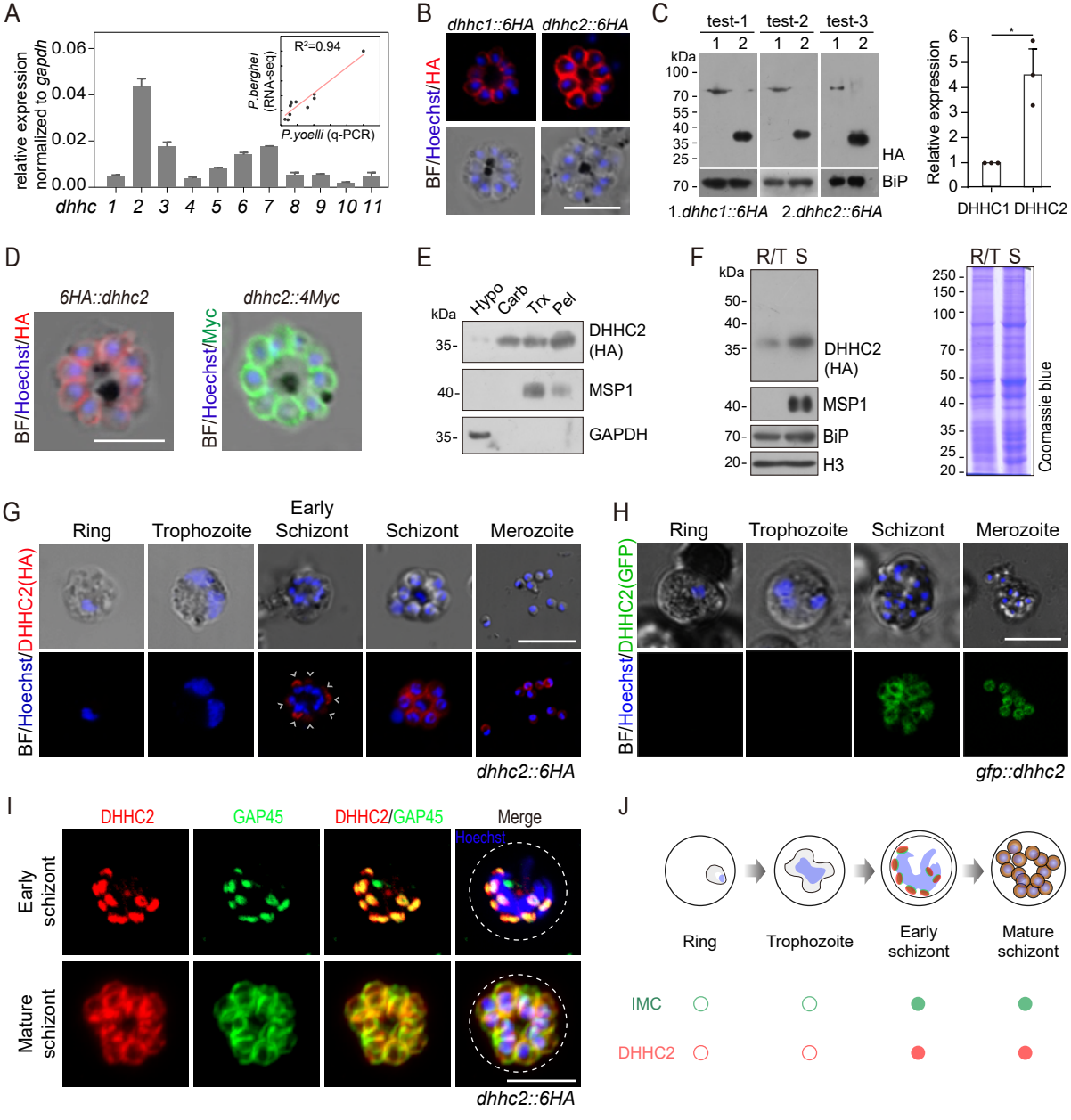
A
relative expression normalized to gapdh
0.06
0.04
0.02
0.00
dhhc 1 2 3 4 5 6 7 8 9 10 11
R²=0.94
P.berghei (RNA-seq)
P.yoelii (q-PCR)
B
dhhc1::6HA
dhhc2::6HA
BF/Hoechst/HA
C
test-1 test-2 test-3
1 2 1 2 1 2
kDa
100
70
55
40
35
25
70
HA
BiP
1.dhhc1::6HA 2.dhhc2::6HA
Relative expression
6
5
4
3
2
1
0
*
DHHC1 DHHC2
D
6HA::dhhc2
dhhc2::4Myc
BF/Hoechst/HA
BF/Hoechst/Myc
E
kDa
Hypo
Carb
Trx
Pel
35-
DHHC2 (HA)
40-
MSP1
35-
GAPDH
F
R/T S
kDa
50-
40-
35-
DHHC2 (HA)
40-
MSP1
70-
BiP
20-
H3
R/T S
250
150
100
70
50
40
35
25
20
Coomassie blue
G
Ring
Trophozoite
Early Schizont
Schizont
Merozoite
BF/Hoechst/DHHC2(HA)
dhhc2::6HA
H
Ring
Trophozoite
Schizont
Merozoite
BF/Hoechst/DHHC2(GFP)
gfp::dhhc2
I
DHHC2
GAP45
DHHC2/GAP45
Merge
Hoechst
Early schizont
Mature schizont
dhhc2::6HA
J
Ring
Trophozoite
Early schizont
Mature schizont
IMC
DHHC2

Figure 4. DHHC2 is an IMC-residing palmitoyl-S-acyl-transferase in schizonts

A. RT-qPCR of transcripts for 11 *dhhc* (*dhhc1- dhhc11*) in schizonts. Gene expression was normalized to the *gapdh* transcript. The inlet indicates positive correlation between mRNA levels of these *P. yoelii dhhc* genes and mRNA levels of their *dhhc* orthologs in *P. berghei* determined via RNA-seq. Values are means ± SD (n=3).

B. IFA analysis of DHHC1 and DHHC2 in schizonts from two tagged parasite strains *dhhc1::6HA* and *dhhc2::6HA*. Scale bar = 5 μm.

C. Immunoblot of DHHC1 and DHHC2 from the cell lysate of similar number of schizonts from the *dhhc1::6HA* and *dhhc2::6HA* parasite respectively. Right panel: the quantification of band intensity. Values are means ± SEM (n = 3 biological replicates), two-tailed t-test, *P < 0.05.

D. IFA analysis of DHHC2 in schizonts of another two tagged parasite strains *6HA::dhhc2* and *dhhc2::4Myc*. Scale bar = 5 μm.

E. Solubility assay detected membrane association of DHHC2 in schizonts using different detergents. Cytosolic soluble proteins are in hypotonic buffer (Hypo), peripheral membrane proteins in carbonate buffer (Carb), integral membrane proteins in Triton X-100 buffer (Trx), and insoluble proteins in pellet (Pel). DHHC2 is in the membrane-associated fractions as IMC protein GAP45 and PM protein MSP1, while cytoplasm protein GAPDH is in the soluble fraction. Two replicates performed.

F. Immunoblot of DHHC2 from early stages containing ring and trophozoite (R/T) and late stages containing schizont (S) of the *dhhc2::6HA* parasites. Merozoite surface protein MSP1 was mainly expressed in the schizonts. BiP, histone H3, and Coomassie blue staining of total lysate were used as loading control. Two replicates performed.

G. DHHC2 expression dynamics in different asexual blood stages (ring, trophozoite, schizont, and merozoite) of the parasite *dhhc2::6HA* by IFA. Scale bar = 5 μm.

H. Fluorescent microscopy of GFP::DHHC2 in different asexual blood stages of the parasites *gfp::dhhc2*. Scale bar = 5 μm.

I. Maximum intensity projections of super-resolution immunofluorescence microscopy (Airyscan) of early and mature *dhhc2::6HA* schizonts stained with anti-HA and anti-GAP45 antibodies. Scale bar = 5 μm.

J. Model showing the IMC-associated localization of DHHC2 in the schizonts.

Figure 5

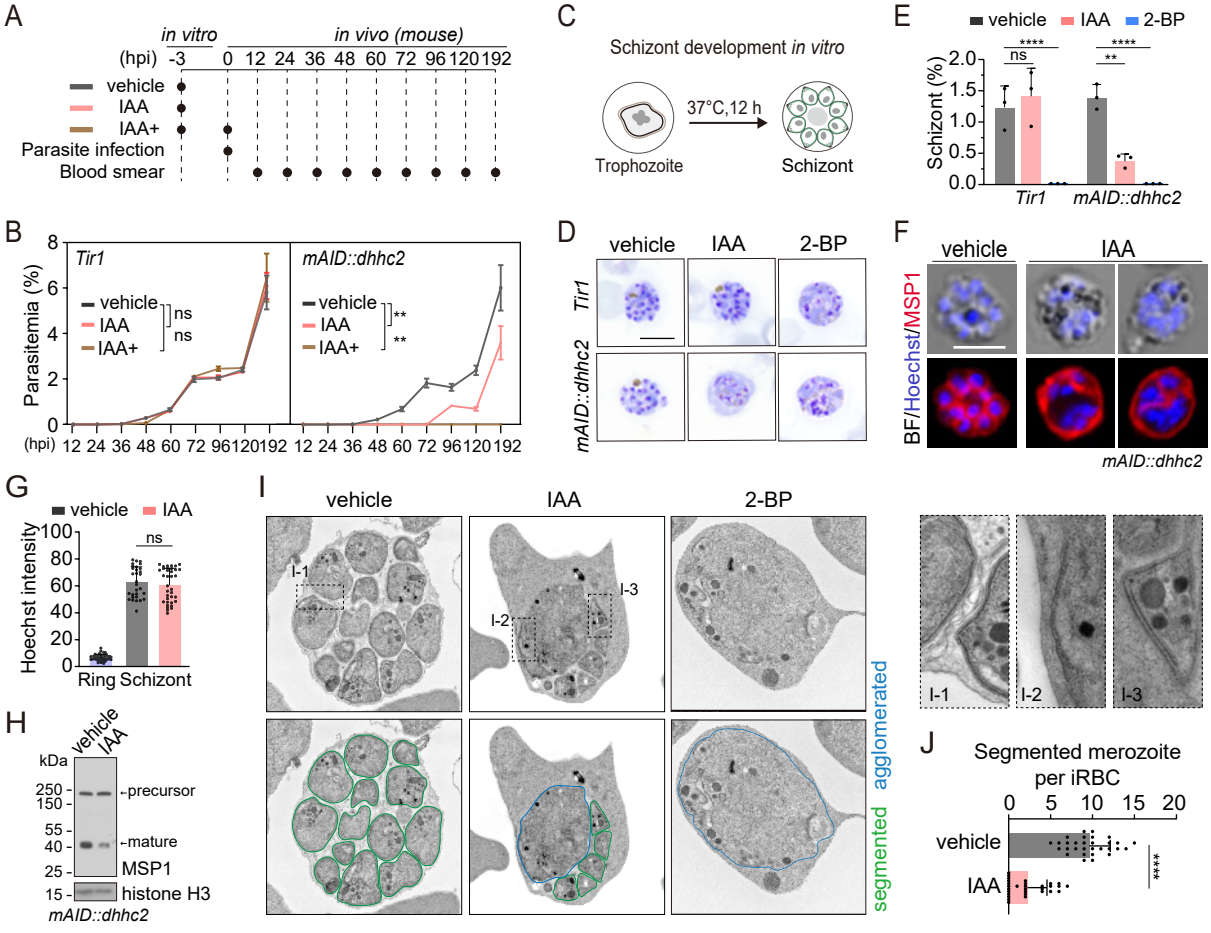
A
in vitro
in vivo (mouse)
(hpi) -3 0 12 24 36 48 60 72 96 120 192
vehicle
IAA
IAA+
Parasite infection
Blood smear
C
Schizont development in vitro
37°C,12 h
Trophozoite
Schizont
E
vehicle
IAA
2-BP
Schizont (%)
ns
****
**
Tir1
mAID::dhhc2
B
Tir1
mAID::dhhc2
Parasitemia (%)
vehicle
IAA
IAA+
ns
**
(hpi) 12 24 36 48 60 72 96 120 192
D
vehicle
IAA
2-BP
Tir1
mAID::dhhc2
F
vehicle
IAA
BF/Hoechst/MSP1
mAID::dhhc2
G
vehicle
IAA
Hoechst intensity
ns
Ring
Schizont
H
vehicle
IAA
kDa
250
150
55
40
25
15
precursor
mature
MSP1
histone H3
mAID::dhhc2
I
vehicle
IAA
2-BP
I-1
I-2
I-3
segmented
agglomerated
J
Segmented merozoite per iRBC
vehicle
IAA
****

Figure 5. DHHC2 is essential for parasite proliferation in mice and regulates schizont segmentation and merozoite invasion

A. Experimental design of *in vivo* test of DHHC2 essentiality using AID. Parasites of *Tir1* and *mAID::dhhc2* were pretreated with vehicle or IAA for 3 h *in vitro*, then intravenously injected to C57BL/6 mice. In the IAA+ treatment group, another IAA injection (200 mg/kg, *ip*) at time of parasite infection was applied for further DHHC2 depletion in *vivo*. From 12 to 192 h post infection, the parasitemia in mice infected with *Tir1* and *mAID::dhhc2* was monitored by blood smear every 12 h.

B. *Tir1* and *mAID::dhhc2* parasite proliferation in mice (n = 3 per group) at each treatment group in **A**.

C. Schematic of the schizont development from trophozoite *in vitro*. Purified early stage parasites containing ring and trophozoite were cultured with vehicle, IAA, or 2-BP for 12 h to mature schizont.

D. Giemsa staining of the schizonts developed from *Tir1* and *mAID::dhhc2* parasites treated with vehicle, IAA, or 2-BP illustrated in **C**. Scale bar = 5 μm.

E. Quantification of mature schizonts in **D**. Values are means ± SEM (n = 3 biological replicates), two-tailed t-test, **P < 0.01, ****P < 0.0001.

F. Co-staining of the *mAID::dhhc2* schizonts in **C** with antibody against merozoite surface protein MSP1 and Hoechst 33342. Scale bar= 5 μm.

G. Quantification of Hoechst signal in schizonts indicating nuclear DNA contents in **F**. More than 30 schizonts were analyzed in each group. Signal in ring stage parasites serves as a control. Values were mean ± SD, Mann Whiteny test applied, ns, not significant.

H. Immunoblot of MSP1 in the schizonts developed from the *mAID::dhhc2* parasites treated with vehicle and IAA. Precursor form (~200 kD) and mature form (~42 kD) of MSP1 were shown. Histone H3 used as a loading control.

I. Representative images of transmission electron microscopy (TEM) of schizonts developed from the *mAID::dhhc2* parasites treated with vehicle, IAA, or 2-BP. Right panels indicate 3 examples of representative daughter cell pellicle including PM and IMC.

J. Quantification of fully segmented merozoites in schizonts in **I**. More than 30 schizonts were analyzed in each group. Values were shown as mean ± SD, Mann Whiteny test, ****P < 0.0001.

Figure 6

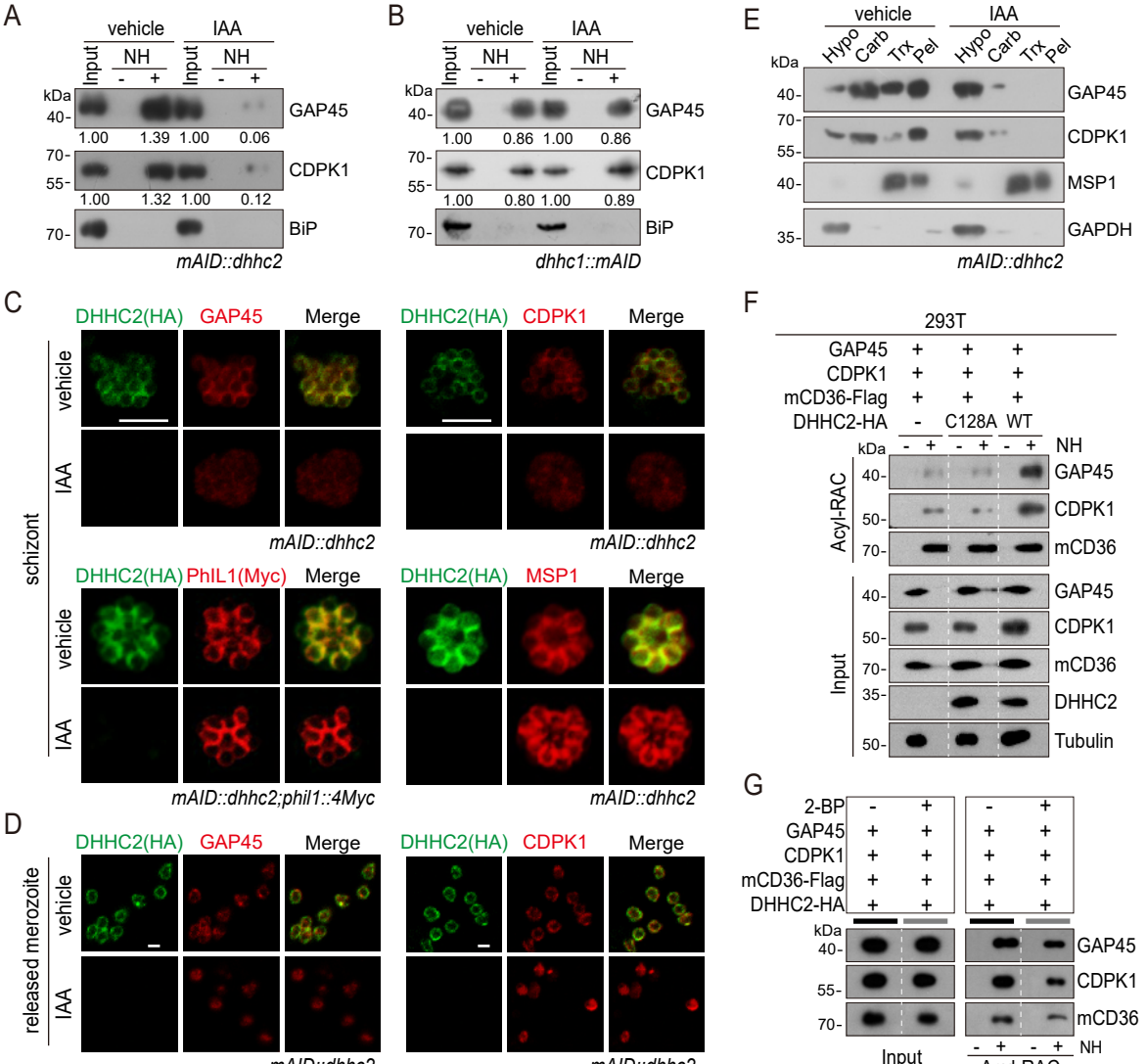
A
vehicle
IAA
Input
NH
kDa
40-
GAP45
1.00 1.39 1.00 0.06
70-
55-
CDPK1
1.00 1.32 1.00 0.12
70-
BiP
mAID::dhhc2
B
vehicle
IAA
Input
NH
kDa
40-
GAP45
1.00 0.86 1.00 0.86
70-
55-
CDPK1
1.00 0.80 1.00 0.89
70-
BiP
dhhc1::mAID
E
vehicle
IAA
Hypo
Carb
Trx
Pel
kDa
40-
GAP45
70-
55-
CDPK1
40-
MSP1
35-
GAPDH
mAID::dhhc2
C
schizont
vehicle
IAA
DHHC2(HA)
GAP45
Merge
CDPK1
PhIL1(Myc)
MSP1
mAID::dhhc2
mAID::dhhc2;phil1::4Myc
D
released merozoite
F
293T
GAP45 + + +
CDPK1 + + +
mCD36-Flag + + +
DHHC2-HA - C128A WT
NH
Acyl-RAC
Input
GAP45
CDPK1
mCD36
DHHC2
Tubulin
G
2-BP - + - +
GAP45 + + + +
CDPK1 + + + +
mCD36-Flag + + + +
DHHC2-HA + + + +
Input
Acyl-RAC

Figure 6. DHHC2 palmitoylates GAP45 and CDPK1 in the schizonts

A. Acyl-RAC method detecting palmitoylation of GAP45 and CDPK1 in the *mAID::dhhc2* schizonts treated with vehicle or IAA. BiP served as a loading control. Two replicates performed.

B. Acyl-RAC method detecting palmitoylation of GAP45 and CDPK1 in the *dhhc1::mAID* schizonts treated with vehicle or IAA. BiP served as a loading control. Two replicates performed.

C. IFA analysis of GAP45, CDPK1, PhIL1, and MSP1 expression in schizonts treated with vehicle or IAA. Parasites *mAID::dhhc2* and *mAID::dhhc2;phil1::4Myc* used are indicated. Scale bar = 5 μm.

D. IFA analysis of GAP45 and CDPK1 in released *mAID::dhhc2* merozoites treated with vehicle or IAA. Scale bar = 5 μm.

E. Solubility assay detected membrane association of GAP45, CDPK1, and MSP1 in the *mAID::dhhc2* schizonts treated with vehicle or IAA. PM protein MSP1 and cytoplasmic protein GAPDH are set as control. Two replicates performed.

F. Palmitoylation analysis of GAP45 and CDPK1 ectopically expressed in human cells. Human embryonic kidney 293T cells were co-transfected with plasmids coding for the HA-tagged and human codon-optimized DHHC2 (WT) or its catalytic-deficient mutant (C128A), along with the GAP45 and CDPK1. Flag-tagged mouse CD36 (mCD36-Flag) was also co-transfected and serves as a control of evidenced palmitoylated protein. Tubulin served as a loading control. Two replicates performed.

G. Palmitoylation analysis of GAP45 and CDPK1 ectopically expressed in human HEK293T cells treated with or without 2-BP. The cells were co-transfected with a HA-tagged and human codon-optimized DHHC2 and a Flag-tagged mouse CD36 (mCD36-Flag). Two replicates performed.

Figure 7

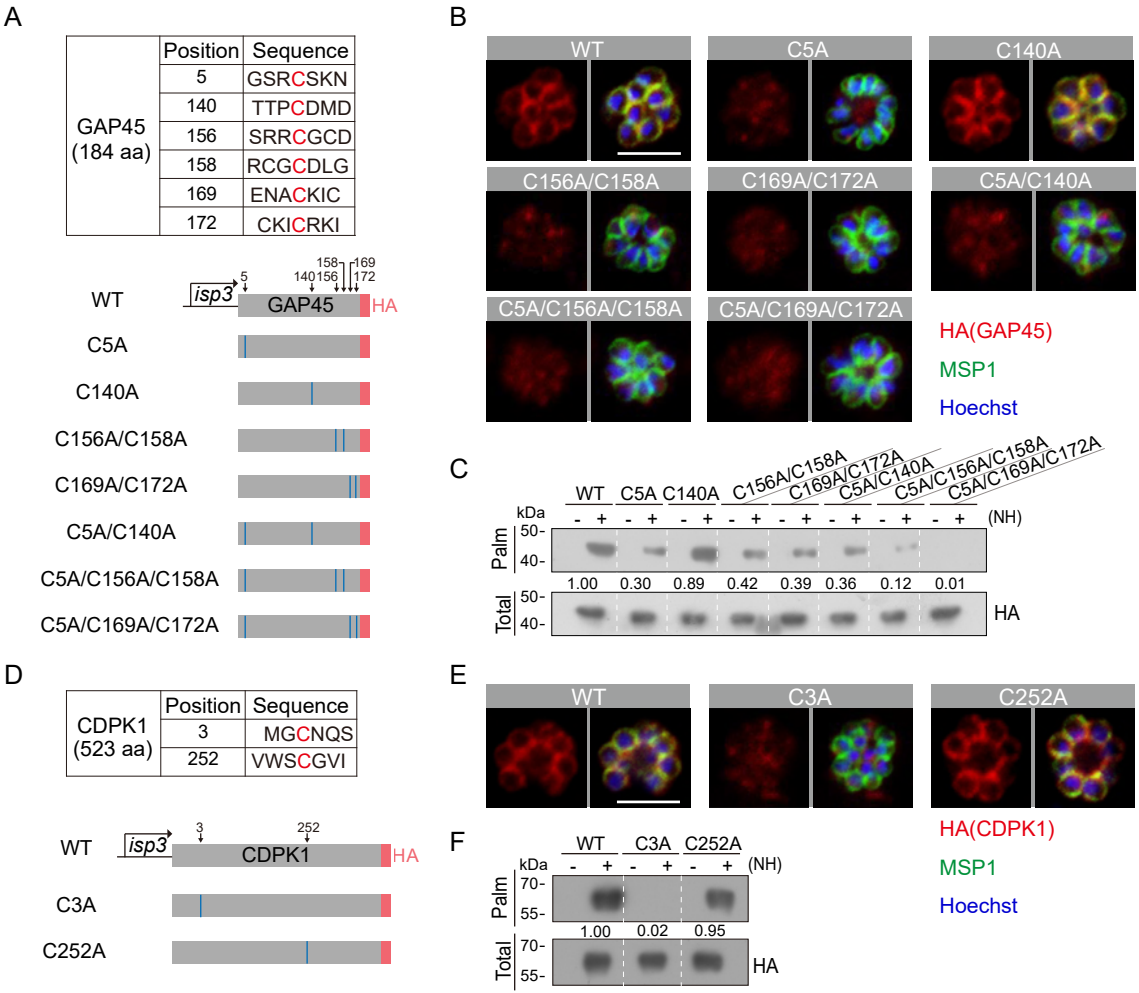
A
GAP45 (184 aa)
Position
Sequence
5
GSRCSKN
140
TTPCDMD
156
SRRCGCD
158
RCGCDLG
169
ENACKIC
172
CKICRKI
WT
C5A
C140A
C156A/C158A
C169A/C172A
C5A/C140A
C5A/C156A/C158A
C5A/C169A/C172A
isp3
GAP45
HA
B
WT
C5A
C140A
C156A/C158A
C169A/C172A
C5A/C140A
C5A/C156A/C158A
C5A/C169A/C172A
HA(GAP45)
MSP1
Hoechst
C
WT C5A C140A C156A/C158A C169A/C172A C5A/C140A C5A/C156A/C158A C5A/C169A/C172A
kDa
(NH)
Palm
Total
50-
40-
1.00 0.30 0.89 0.42 0.39 0.36 0.12 0.01
HA
D
CDPK1 (523 aa)
Position
Sequence
3
MGCNQS
252
VWSCGVI
WT
C3A
C252A
isp3
CDPK1
HA
E
WT
C3A
C252A
HA(CDPK1)
MSP1
Hoechst
F
WT C3A C252A
kDa
(NH)
Palm
Total
70-
55-
1.00 0.02 0.95
HA

Figure 7. Residues for palmitoylation in GAP45 and CDPK1

A. 6 cysteine predicated for palmitoylation in GAP45 (upper panel). Lower panels indicate schematic of constructs expressing HA-tagged GAP45, each with a cysteine to alanine replacement in single, double, or triple residues (C5A, C140A, C156A/C158A, C169A/C172A, C5A/C140A, C5A/C156A/C158A, and C5A/C169A/C172A). These constructs were episomally expressed in the schizonts.

B. IFA of GAP45::HA and 7 mutant proteins episomally expressed in schizonts. Scale bar = 5 μm. Representative of 3 independent repeats.

C. Palmitoylation analysis of GAP45::HA and 7 mutant proteins episomally expressed in schizonts. Representative of two independent repeats.

D. 2 cysteine predicated for palmitoylation in CDPK1 (upper panel). Lower panels indicate schematic of constructs expressing HA-tagged CDPK1, each with a cysteine to alanine replacement in single residue (C3A and C252A). These constructs were episomally expressed in the schizonts.

E. IFA of CDPK1::HA and 2 mutant proteins episomally expressed in schizonts. Scale bar = 5 μm. Representative of 3 independent repeats.

F. Palmitoylation analysis of CDPK1::HA and 2 mutant proteins episomally expressed in schizonts. Representative of two independent repeats.

Supplemental Information

Inner membrane complex proteomics reveals a palmitoylation cascade regulating intraerythrocytic development of malaria parasite

Pengge Qian [1, 4], Xu Wang[1, 4], Chuan-Qi Zhong[1, 4], Jiaxu Wang[2, 4], Mengya Cai[1], Wang Nguitragool[3], Jian Li [1,*], Huiting Cui [1,*], Jing Yuan[1,*]

1. Supplementary Figures 1-9 and figure legends

2. Table S1. List of IMC proteins identified in this study

3. Table S2. Primers and oligonucleotides used in this study

Figure S1

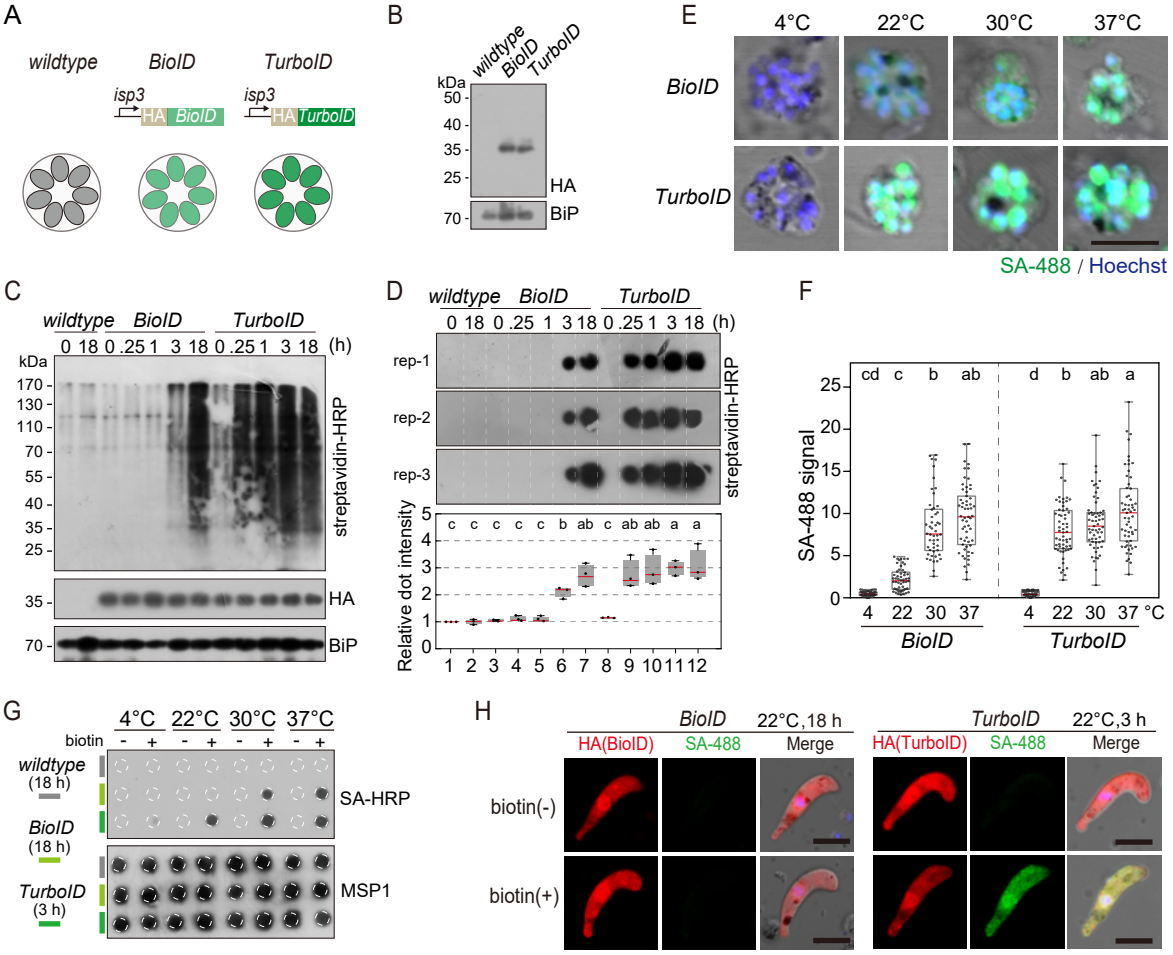
A
wildtype
BioID
TurboID
isp3
HA
BioID
isp3
HA
TurboID
B
wildtype
BioID
TurboID
kDa
50
40
35
25
70
HA
BiP
E
4°C
22°C
30°C
37°C
BioID
TurboID
SA-488 / Hoechst
C
wildtype
BioID
TurboID
0 18 0 .25 1 3 18 0 .25 1 3 18 (h)
kDa
170
130
110
70
55
40
35
25
streptavidin-HRP
35
HA
70
BiP
D
wildtype
BioID
TurboID
0 18 0 .25 1 3 18 0 .25 1 3 18 (h)
rep-1
rep-2
rep-3
streptavidin-HRP
Relative dot intensity
c c c c c b ab c ab ab a a
1 2 3 4 5 6 7 8 9 10 11 12
F
SA-488 signal
cd c b ab d b ab a
4 22 30 37 4 22 30 37 °C
BioID
TurboID
G
4°C
22°C
30°C
37°C
biotin
- + - + - + - +
wildtype
(18 h)
BioID
(18 h)
TurboID
(3 h)
SA-HRP
MSP1
H
BioID
22°C,18 h
HA(BioID)
SA-488
Merge
TurboID
22°C,3 h
HA(TurboID)
SA-488
Merge
biotin(-)
biotin(+)

Supplementary Figure 1. Protein proximity labelling by biotin ligases BioID and TurboID in the *P. yoelii* parasites

A. Schematic of the expressing cassettes for transient expression of BioID and TurboID. The ligase was fused with a HA and driven by the promoter of the *isp3* gene.

B. Immunoblot of the HA-tagged ligases episomally expressed in the asexual blood stages of the *P. yoelii*. BiP as the loading control.

C. Streptavidin blot detecting the biotinylated proteins from the wildtype, BioID or TurboID-expressing parasites incubated with exogenous biotin for different time (0, 0.25, 1, 3, and 18 h) at 37°C. ER protein BiP is a loading control.

D. Streptavidin dot blot of the biotinylated proteins from total lysate of parasites in **C**. Low panel shows the quantification of dot signals. Signals of wildtype parasite at 0 h are set as 1.0, red bars indicate mean value. Different letters above the boxes indicate significant difference with a $p < 0.05$. ANOVA analysis, followed by Tukey's multiple comparison tests (n = 3 biological replicates).

E. IFA of the biotinylated proteins in the schizonts from the BioID or TurboID-expressing parasites incubated at different temperature (4, 22, 30, and 37°C). Wildtype and BioID parasites were incubated with biotin for 18 h while TurboID parasites were incubated with biotin for 3 h. Parasites were stained with the Alexa Fluor 488 conjugated streptavidin (SA-488). Scale bar=5 μm.

F. Quantitation of IFA signal intensity in **E**. In each group, at least 30 parasite cells were counted. The signals were shown in the box-and-whisker plot and red bars indicate mean value. Different letters above the boxes indicate significant difference with a $p < 0.05$. ANOVA analysis, followed by Tukey's multiple comparison tests (n = 3 biological replicates).

G. Streptavidin dot blot of the biotinylated proteins from the parasite lysates in **E**. Merozoite surface protein MSP1 is used as the loading control.

H. IFA detecting the biotinylated proteins in the ligase-expressing ookinetes with or without biotin inoculation at 22°C. Cultured ookinetes expressing BioID and TurboID ligase were incubated for 18 or 3 h respectively, with or without 100 μM biotin at 22°C. The ookinetes were co-stained with the SA-488 and anti-HA antibody. Scale bar=5 μm.

Figure S2

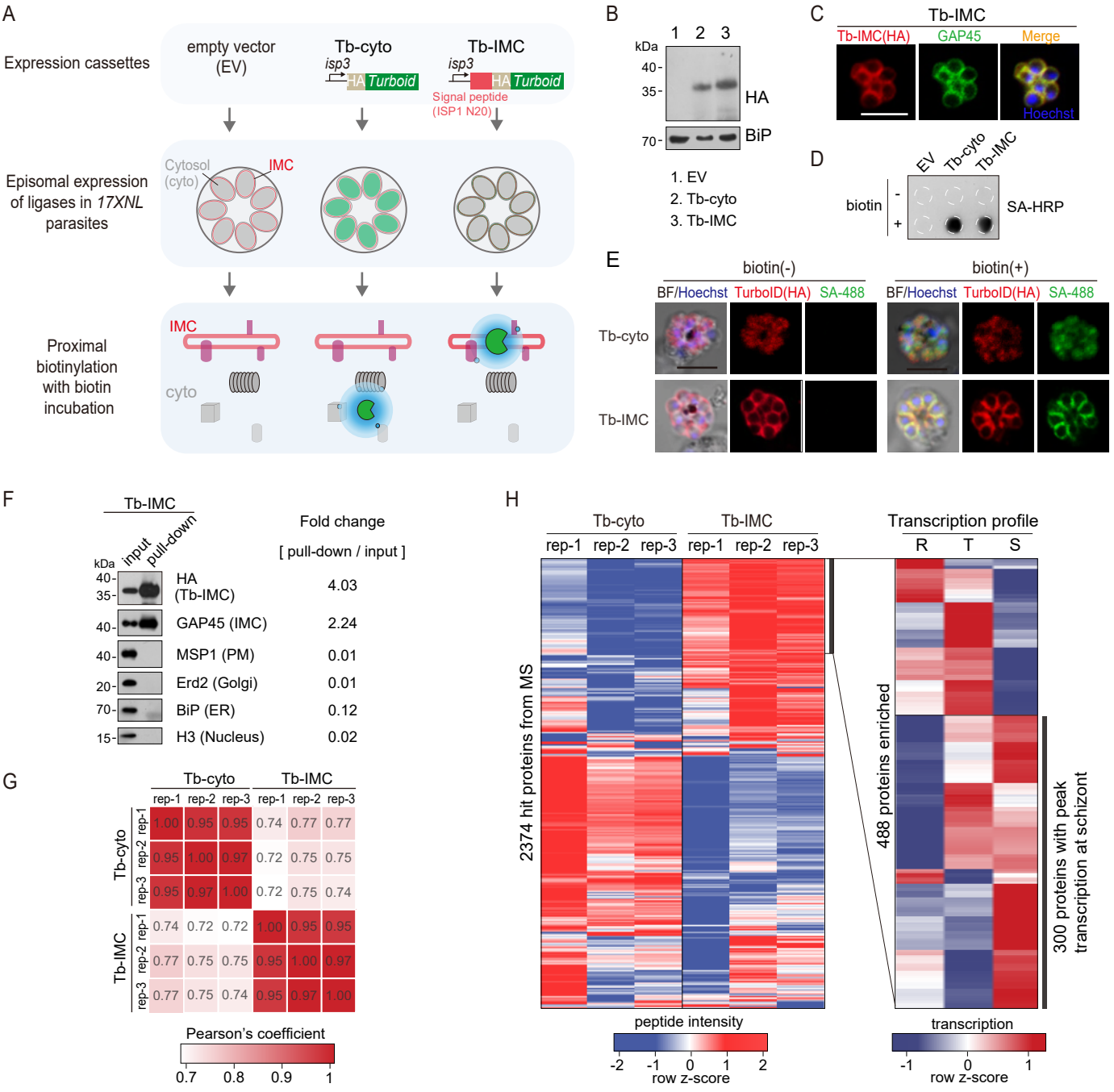
A
Expression cassettes
empty vector (EV)
Tb-cyto
isp3
HA Turboid
Tb-IMC
isp3
HA Turboid
Signal peptide (ISP1 N20)
Episomal expression of ligases in 17XNL parasites
Cytosol (cyto)
IMC
Proximal biotinylation with biotin incubation
IMC
cyto
B
kDa
1 2 3
40-
35-
HA
70-
BiP
1. EV
2. Tb-cyto
3. Tb-IMC
C
Tb-IMC
Tb-IMC(HA)
GAP45
Merge
Hoechst
D
EV
Tb-cyto
Tb-IMC
biotin
-
+
SA-HRP
E
biotin(-)
biotin(+)
BF/Hoechst
TurboID(HA)
SA-488
Tb-cyto
Tb-IMC
F
Tb-IMC
input
pull-down
kDa
40-
35-
HA (Tb-IMC)
40-
GAP45 (IMC)
40-
MSP1 (PM)
20-
Erd2 (Golgi)
70-
BiP (ER)
15-
H3 (Nucleus)
Fold change
[pull-down / input]
4.03
2.24
0.01
0.01
0.12
0.02
G
Tb-cyto
Tb-IMC
rep-1
rep-2
rep-3
1.00 0.95 0.95 0.74 0.77 0.77
0.95 1.00 0.97 0.72 0.75 0.75
0.95 0.97 1.00 0.72 0.75 0.74
0.74 0.72 0.72 1.00 0.95 0.95
0.77 0.75 0.75 0.95 1.00 0.97
0.77 0.75 0.74 0.95 0.97 1.00
Pearson's coefficient
0.7 0.8 0.9 1
H
Tb-cyto
Tb-IMC
rep-1 rep-2 rep-3 rep-1 rep-2 rep-3
Transcription profile
R T S
2374 hit proteins from MS
488 proteins enriched
300 proteins with peak transcription at schizont
peptide intensity
-2 -1 0 1 2
row z-score
transcription
-1 0 1
row z-score

Supplementary Figure 2. TurboID-mediated labelling of IMC proteins in the schizonts

A. Experimental workflow for TurboID proximity labeling of the IMC proteins in the schizont. The HA-tagged TurboID is fused with an IMC signal peptide, the N-terminal 20 residues of ISP1 (Tb-IMC). The HA-tagged TurboID alone (Tb-cyto) serves as a control for non-specific biotinylation. Both ligases (Tb-IMC and Tb-cyto) were driven by the promoter of gene *isp3* and episomally expressed in the asexual blood stages. The schizonts expressing Tb-IMC, Tb-cyto, or empty vector (EV: construct without ligase gene) were purified and cultivated with 100 μM biotin at 37°C for 3 h.

B. Immunoblot of the HA-tagged ligase from the total lysate of schizonts expressing the Tb-cyto or Tb-IMC shown in **A**. ER protein BiP used as a loading control.

C. IFA of the Tb-IMC expressing schizonts with anti-HA antibody, anti-GAP45 antibody, and DNA stain Hoechst 33342. Scale bar=5 μm.

D. Streptavidin dot blot of biotinylated proteins in the EV, Tb-cyto, Tb-IMC expressing schizonts incubated with or without 100 μM biotin.

E. Co-staining of TurboID ligase and biotinylated proteins in the schizonts expressing the Tb-cyto or Tb-IMC. The schizonts incubated with or without 100 μM biotin were co-stained with anti-HA antibody and streptavidin-488 (SA-488). Scale bar=5 μm.

F. Immunoblot of streptavidin-affinity purified biotinylated proteins in Tb-IMC schizonts. Tb-IMC ligase and several organelle marker proteins were probed with the indicated antibodies. Relative band intensity of each protein in the pull-down compared to the input indicates the enrichment ratio.

G. Correlation analysis of change in protein abundance among biological replicates between Tb-cyto and Tb-IMC. Three biological replicates were prepared from Tb-IMC and Tb-cyto schizonts, and the streptavidin-affinity purified proteins were for proteomic analysis by MS.

H. Identification of 300 Tb-IMC interacting protein by quantitative MS and comparative transcription profiling. Clustered heatmap (left panel) of MS peptide intensity revealed 488 enriched proteins with high confidence (an adjusted P value < 0.05) in Tb-IMC compared to Tb-cyto. Comparative analysis of transcription pattern (right panel) based on the *P. berghei* transcriptome further narrow the candidates to 300 proteins, in which many known IMC or IMC-associated proteins were indicated. R: ring, T: trophozoite, and S: schizont.

Figure S3

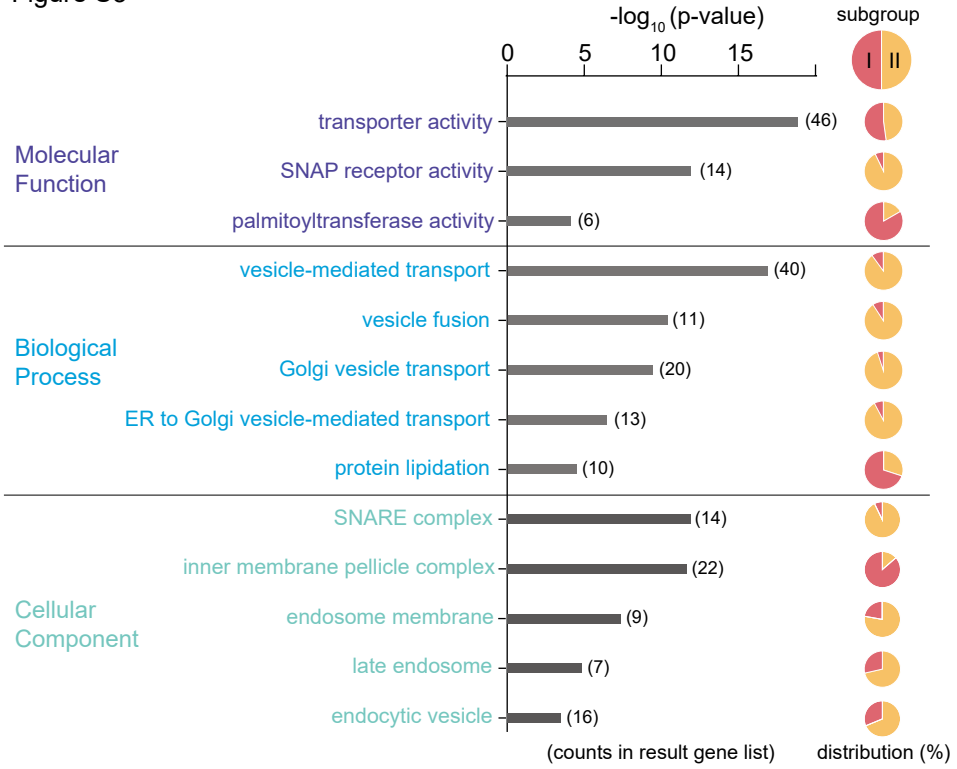
-log10 (p-value)
0
5
10
15
subgroup
I
II
Molecular Function
transporter activity
(46)
SNAP receptor activity
(14)
palmitoyltransferase activity
(6)
Biological Process
vesicle-mediated transport
(40)
vesicle fusion
(11)
Golgi vesicle transport
(20)
ER to Golgi vesicle-mediated transport
(13)
protein lipidation
(10)
Cellular Component
SNARE complex
(14)
inner membrane pellicle complex
(22)
endosome membrane
(9)
late endosome
(7)
endocytic vesicle
(16)
(counts in result gene list)
distribution (%)

Supplementary Figure 3. Predicated functional profile of the Tb-IMC interacting proteins

Gene ontology analysis of the 300 Tb-IMC interacting proteins. Bar plot showing the significantly enriched GO terms from "Molecular Function" (top panel), "Biological Process" (middle panel) and "Cellular Component" (bottom panel). For each of GO terms, the distribution of proteins from the subgroup I and II was indicated in the pie chart.

Figure S4

A

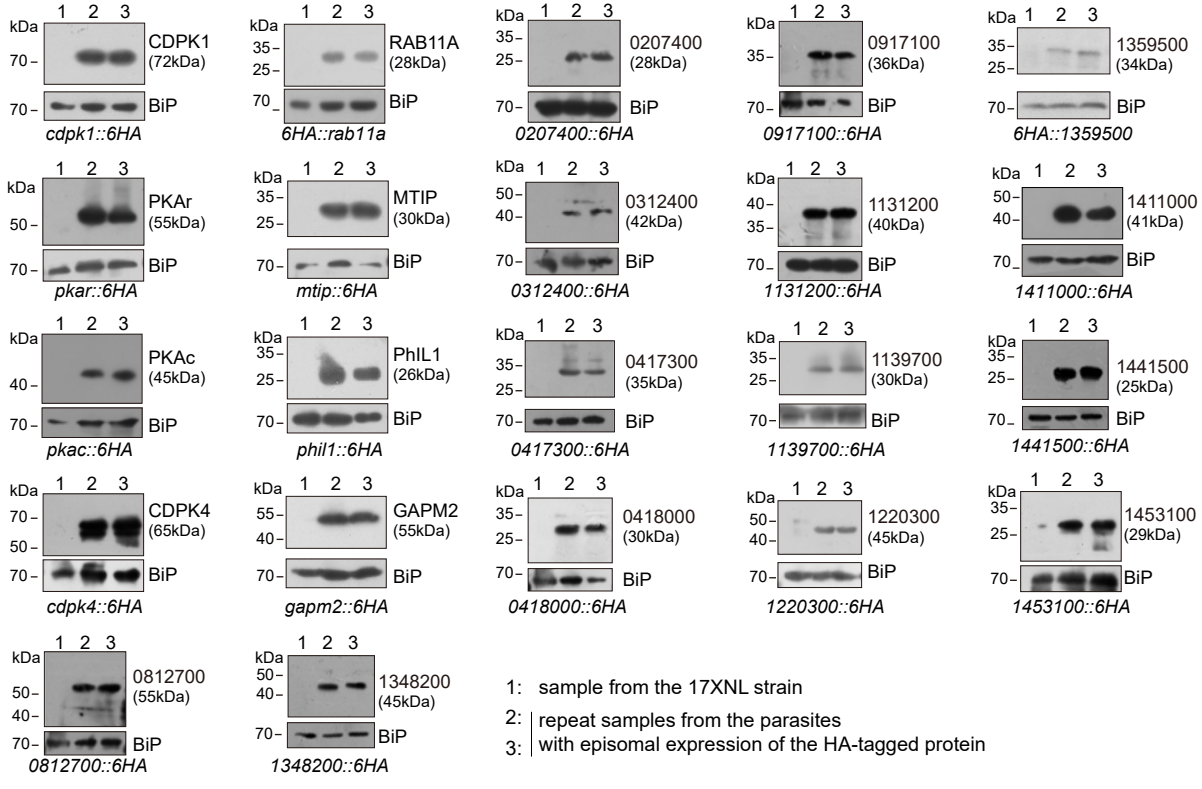
kDa 1 2 3
CDPK1 (72kDa)
BiP
cdpk1::6HA
RAB11A (28kDa)
6HA::rab11a
0207400 (28kDa)
0207400::6HA
0917100 (36kDa)
0917100::6HA
1359500 (34kDa)
6HA::1359500
PKAr (55kDa)
pkar::6HA
MTIP (30kDa)
mtip::6HA
0312400 (42kDa)
0312400::6HA
1131200 (40kDa)
1131200::6HA
1411000 (41kDa)
1411000::6HA
PKAc (45kDa)
pkac::6HA
PhIL1 (26kDa)
phil1::6HA
0417300 (35kDa)
0417300::6HA
1139700 (30kDa)
1139700::6HA
1441500 (25kDa)
1441500::6HA
CDPK4 (65kDa)
cdpk4::6HA
GAPM2 (55kDa)
gapm2::6HA
0418000 (30kDa)
0418000::6HA
1220300 (45kDa)
1220300::6HA
1453100 (29kDa)
1453100::6HA
0812700 (55kDa)
0812700::6HA
1348200 (45kDa)
1348200::6HA
1: sample from the 17XNL strain
2: repeat samples from the parasites
3: with episomal expression of the HA-tagged protein

B

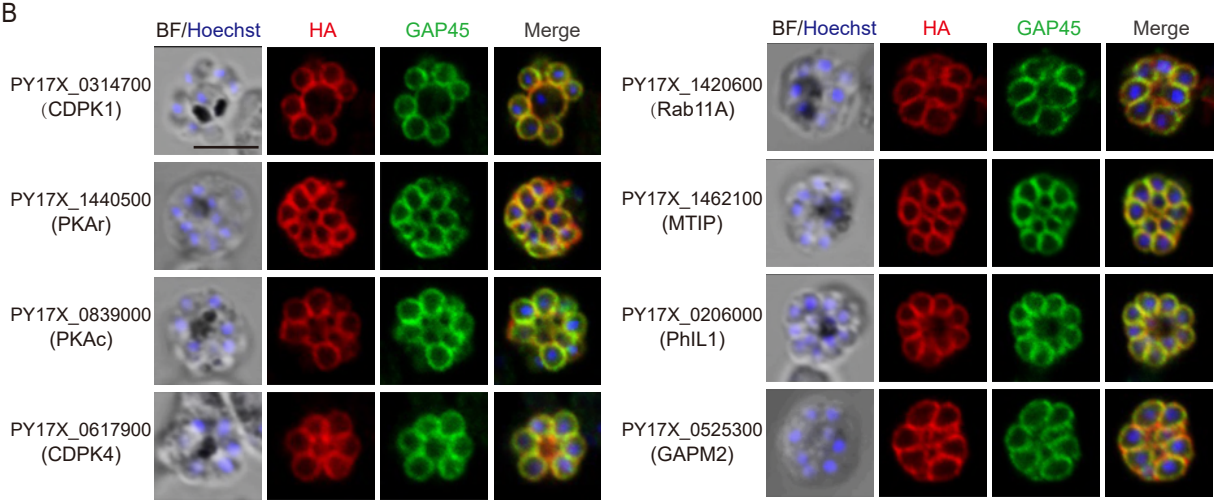
BF/Hoechst
HA
GAP45
Merge
PY17X_0314700 (CDPK1)
PY17X_1440500 (PKAr)
PY17X_0839000 (PKAc)
PY17X_0617900 (CDPK4)
PY17X_1420600 (Rab11A)
PY17X_1462100 (MTIP)
PY17X_0206000 (PhIL1)
PY17X_0525300 (GAPM2)

Supplementary Figure 4. Expression and localization analysis of IMC protein candidates selected in this study

A. Immunoblot of 22 IMC protein candidates in the schizonts of *P. yoelii*. Each candidate protein was tagged with a 6HA at the N- or C-terminus and episomally expressed in the schizonts. BiP as the loading control.

B. IFA of 8 known IMC proteins in the *P. yoelii* schizonts. The orthologues of 8 proteins, including CDPK1, CDPK4, PKAr, PKAc, Rab11A, MTIP, PhIL1, and GAPM2, have been experimentally validated to be IMC-residing in the schizonts of *P. berghei* or *P. falciparum*. Each protein was tagged with a 6HA at the N- or C-terminus and episomally expressed in the schizonts. The schizonts were co-stained with antibodies against GAP45 and HA. Nuclei were stained with Hoechst 33342. Scale bar=5 μm.

Figure S5

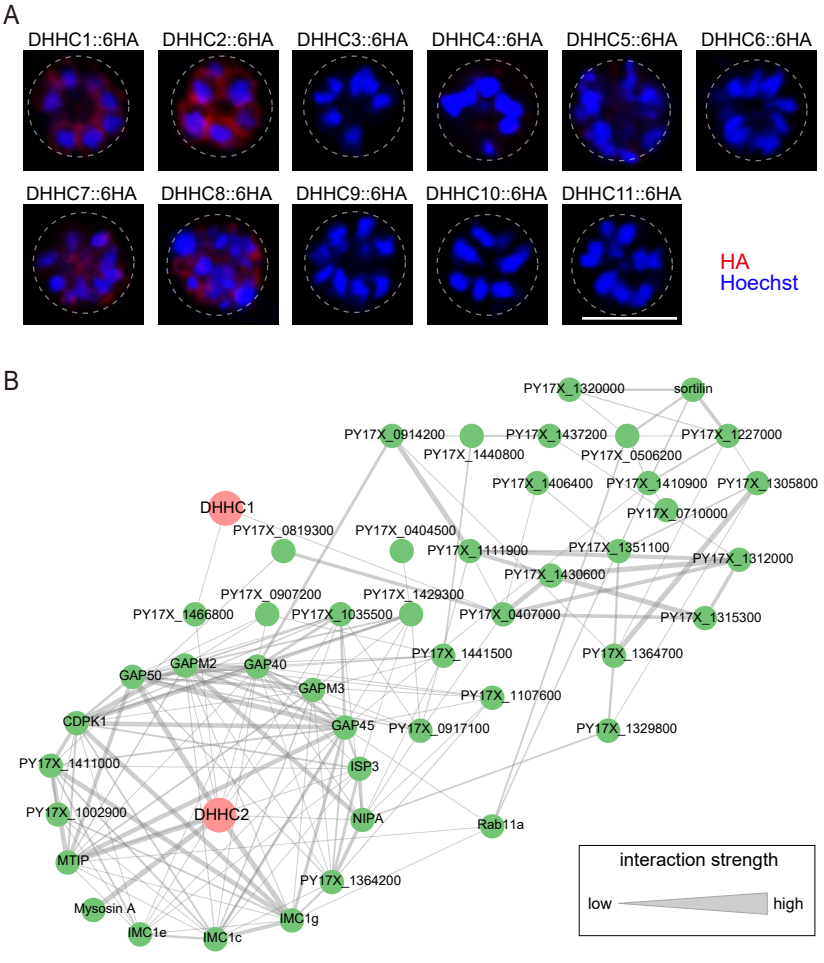
A
DHHC1::6HA
DHHC2::6HA
DHHC3::6HA
DHHC4::6HA
DHHC5::6HA
DHHC6::6HA
DHHC7::6HA
DHHC8::6HA
DHHC9::6HA
DHHC10::6HA
DHHC11::6HA
HA
Hoechst
B
PY17X_1320000
sortilin
PY17X_0914200
PY17X_1437200
PY17X_1227000
PY17X_1440800
PY17X_0506200
PY17X_1406400
PY17X_1410900
PY17X_1305800
DHHC1
PY17X_0710000
PY17X_0819300
PY17X_0404500
PY17X_1111900
PY17X_1351100
PY17X_1312000
PY17X_1430600
PY17X_0907200
PY17X_1429300
PY17X_1466800
PY17X_1035500
PY17X_0407000
PY17X_1315300
PY17X_1441500
PY17X_1364700
GAP50
GAPM2
GAP40
GAPM3
PY17X_1107600
CDPK1
GAP45
PY17X_0917100
PY17X_1329800
PY17X_1411000
ISP3
PY17X_1002900
DHHC2
NIPA
Rab11a
MTIP
PY17X_1364200
Mysosin A
IMC1g
IMC1e
IMC1c
interaction strength
low
high

Supplementary Figure 5. Localization analysis of 11 PATs (DHHC1-11) in schizonts

A. IFA analysis of 11 PATs (DHHC1-11) expression in the schizonts. Each of individual *P. yoelii* PATs was endogenously tagged with a 6HA in the transgenic strains generated previously. The schizonts were co-stained with the anti-HA antibody and Hoechst 33342. Scale bar = 5 μm.

B. Predicted protein interaction network between DHHC1/DHHC2 and the putatively palmitoylated Tb-IMC interacting proteins (STRING; $p < 1.0e-16$).

Figure S6

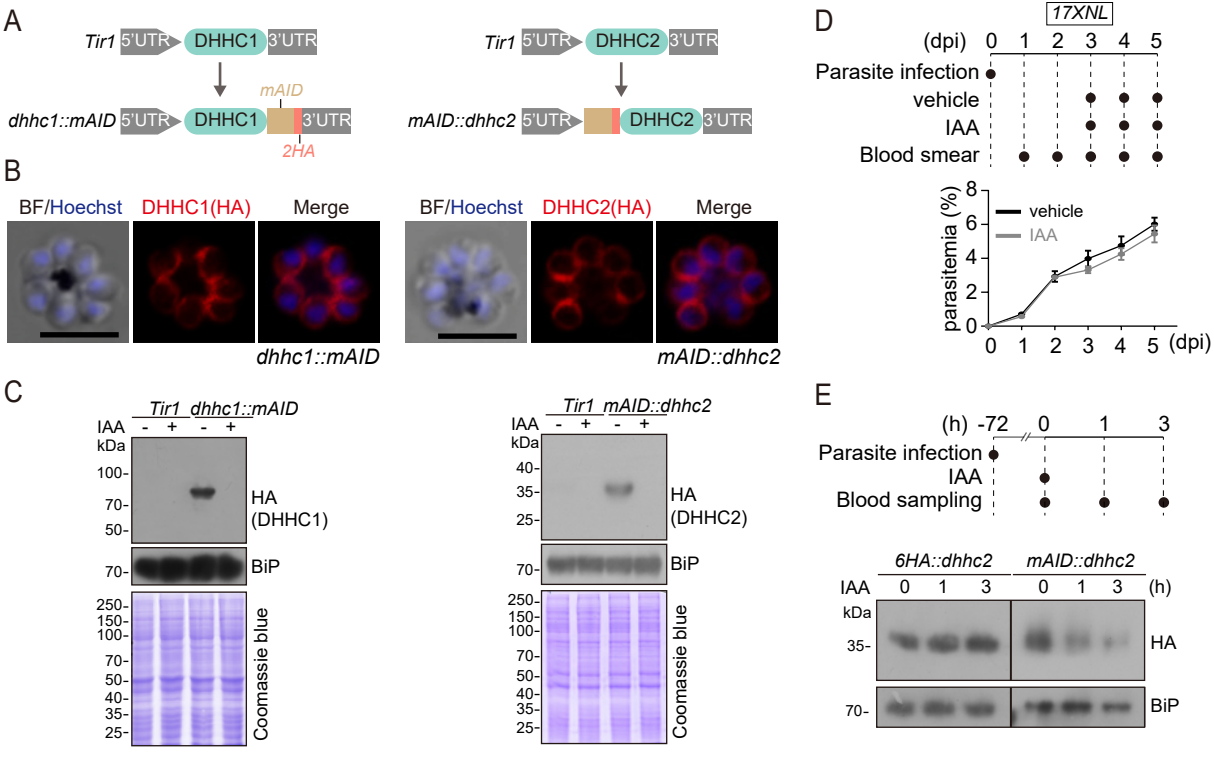
A
Tir1 5'UTR DHHC1 3'UTR
dhhc1::mAID 5'UTR DHHC1 mAID 2HA 3'UTR
Tir1 5'UTR DHHC2 3'UTR
mAID::dhhc2 5'UTR DHHC2 3'UTR
B
BF/Hoechst
DHHC1(HA)
Merge
dhhc1::mAID
BF/Hoechst
DHHC2(HA)
Merge
mAID::dhhc2
C
Tir1 dhhc1::mAID
IAA - + - +
kDa
100-
70-
50-
HA (DHHC1)
70-
BiP
250-
150-
100-
70-
50-
40-
35-
25-
Coomassie blue
Tir1 mAID::dhhc2
IAA - + - +
kDa
40-
35-
25-
HA (DHHC2)
70-
BiP
250-
150-
100-
70-
50-
40-
35-
25-
Coomassie blue
D
17XNL
(dpi) 0 1 2 3 4 5
Parasite infection
vehicle
IAA
Blood smear
parasitemia (%)
8
6
4
2
0
vehicle
IAA
0 1 2 3 4 5 (dpi)
E
(h) -72 0 1 3
Parasite infection
IAA
Blood sampling
6HA::dhhc2
mAID::dhhc2
IAA 0 1 3 0 1 3 (h)
kDa
35-
HA
70-
BiP

Supplementary Figure 6. Generation and characterization of the modified strains with endogenous DHHC2 and DHHC2 tagged with a mAID motif for induced degradation.

A. Schematic of generation of modified strains with endogenous DHHC1 and DHHC2 tagged with a mAID motif for induced degradation by IAA. A mAID::2HA was inserted in-frame to the C-terminus of endogenous DHHC1 and N-terminus of endogenous DHHC2 in the parental parasite *Tir1* using the CRISPR/Cas9 method, generating the strains *dhhc1::mAID* and *mAID::dhhc2* respectively. mAID: mini auxin-inducible degron.

B. IFA of the fusion proteins DHHC1::mAID (left panel) and mAID::DHHC2 (right panel) in the schizonts of *dhhc1::mAID* and *mAID::dhhc2* parasites. Scale bar = 5 μm.

C. Immunoblot of fusion proteins DHHC1::mAID (left panel) and mAID::DHHC2 (right panel) in the schizonts of the *Tir1, dhhc1::mAID* and *mAID::dhhc2* parasites treated with vehicle or IAA (1 mM) for 3 h. BiP and Coomassie blue staining were used as the loading control.

D. Proliferation assessment of wildtype parasite in mice treated with IAA. Upper panel indicates the experimental design. C57BL/6 mice with ~2-3% parasitemia of wildtype parasite (*17XNL*) were injected intraperitoneally with 200 mg/kg/day IAA or vehicle each day for three days (day 3 to 5). Parasitemia was monitored by Giemsa staining of blood smear at indicated time.

E. IAA-induced degradation assessment of parasite mAID::DHHC2 protein in mice. Upper panel indicates the experimental design. C57BL/6 mice with ~10% parasitemia of *mAID::dhhc2* or *6HA::dhhc2* parasites were injected intraperitoneally with IAA (200 mg/kg) for one time and the parasite-infected red blood cells were collected for detecting the protein abundance by immunoblot at different time post IAA injection. BiP was used as a loading control.

Figure S7

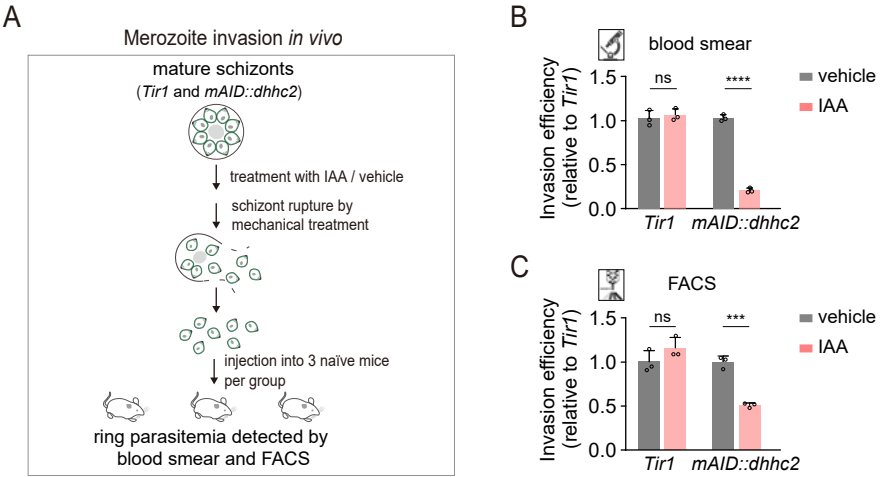
A
Merozoite invasion *in vivo*
mature schizonts
(*Tir1* and *mAID::dhhc2*)
treatment with IAA / vehicle
schizont rupture by
mechanical treatment
injection into 3 naïve mice
per group
ring parasitemia detected by
blood smear and FACS
B
blood smear
Invasion efficiency
(relative to *Tir1*)
1.5
1.0
0.5
0.0
ns
****
vehicle
IAA
Tir1
mAID::dhhc2
C
FACS
Invasion efficiency
(relative to *Tir1*)
1.5
1.0
0.5
0.0
ns
***
vehicle
IAA
Tir1
mAID::dhhc2

Supplementary Figure 7. DHHC2 depletion impaired merozoite invasion.

A. Schematic of merozoite invasion in the mouse. Purified mature schizonts of *Tir1* and *mAID::dhhc2* parasites were pre-treated with IAA for 3 h for protein depletion. Followed by mechanical treatment of schizont for rupture, the released merozoites were collected and injected intravenously into 3 naïve mice per condition. 20 min post-injection, the ability of merozoite invasion was evaluated by counting the parasitemia (ring stage parasite) using blood smear and flow cytometry.

B, C. Histogram showing the invasion efficiency of merozoite in the mice acquired by blood smear (**B**) and flow cytometry (**C**). Invasion efficiency of vehicle-treated group was set as 1.0. Values were mean ± SD, two-tailed t-test, ***P < 0.001, ns, not significant.

Figure S8

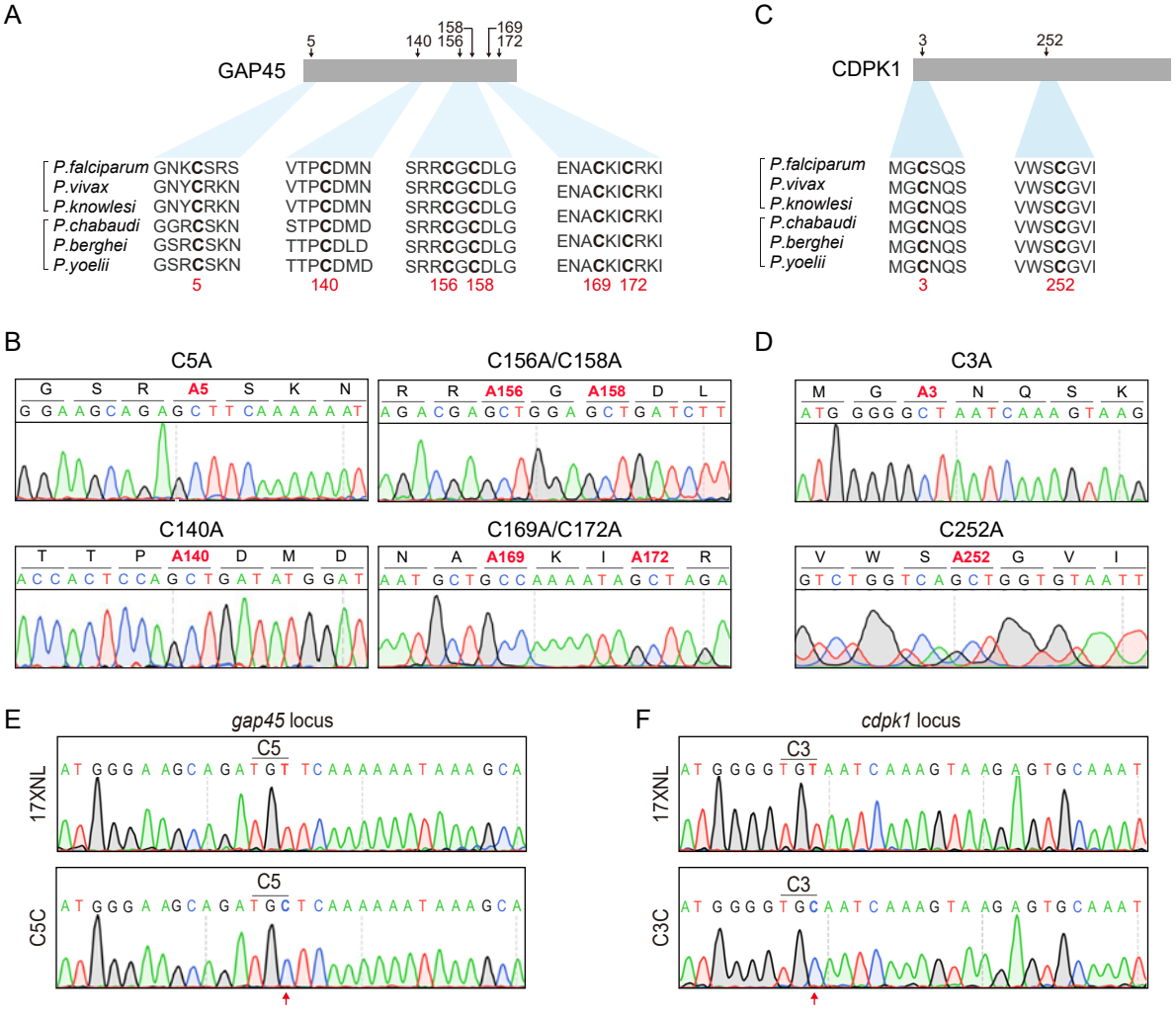
A
GAP45
5
140
158
156
169
172
P.falciparum GNKCSRS VTPCDMN SRRCGCDLG ENACKICRKI
P.vivax GNYCRKN VTPCDMN SRRCGCDLG ENACKICRKI
P.knowlesi GNYCRKN VTPCDMN SRRCGCDLG ENACKICRKI
P.chabaudi GGRCSKN STPCDMD SRRCGCDLG ENACKICRKI
P.berghei GSRCSKN TTPCDLD SRRCGCDLG ENACKICRKI
P.yoelii GSRCSKN TTPCDMD SRRCGCDLG ENACKICRKI
5 140 156 158 169 172
C
CDPK1
3
252
P.falciparum MGCSQS VWSCGVI
P.vivax MGCNQS VWSCGVI
P.knowlesi MGCNQS VWSCGVI
P.chabaudi MGCNQS VWSCGVI
P.berghei MGCNQS VWSCGVI
P.yoelii MGCNQS VWSCGVI
3 252
B
C5A
C156A/C158A
C140A
C169A/C172A
D
C3A
C252A
E
gap45 locus
17XNL
C5C
C5
F
cdpk1 locus
C3C
C3

Supplementary Figure 8. Potential cysteine(s) in GAP45 and CDPK1 for palmitoylation and protein mutants with cysteine replacement to validate the essentiality

A. Amino acid sequence of GAP45 from *P. falciparum* (PF3D7_1222700), *P. vivax* (PVX_123765), *P. knowlesi* (PKNH_1441800), *P. chabaudi* (PCHAS_1439600), *P. berghei* (PBANKA_1437600), and *P. yoelii* (PY17X_1440100) were aligned. 6 conserved cysteine (highlighted in bold) predicated for palmitoylation was shown.

B. DNA sequencing confirmation of the constructs expressing HA-tagged GAP45, each with a cysteine to alanine replacement in single or double residues (C5A, C140A, C156A/C158A, and C169A/C172A). These constructs were episomally expressed in the schizonts.

C. Amino acid sequence of CDPK1 from *P. falciparum* (PF3D7_0217500), *P. vivax* (PVX_002665), *P. knowlesi* (PKNH_0403400), *P. chabaudi* (PCHAS_0316300), *P. berghei* (PBANKA_0314200), and *P. yoelii* (PY17X_0314700) were aligned. 2 conserved cysteine (highlighted in bold) predicated for palmitoylation was shown.

D. DNA sequencing confirmation of the constructs expressing HA-tagged CDPK1, each with a cysteine to alanine replacement (C3A and C252A). These constructs were episomally expressed in the schizonts.

E. DNA sequencing confirmation of nucleotide replacement in the *gap45* locus of the GAP45 C5C parasite clone. Top panel shows the nucleotide sequence from the parasite 17XNL strain; the bottom panel shows the replaced nucleotide (silent mutation) in the clone GAP45 C5C.

F. DNA sequencing confirmation of nucleotide replacement in the *gcdpk1* locus of CDPK1 C3C parasite clone. Top panel shows the nucleotide sequence from the parasite 17XNL strain; the bottom panel shows the replaced nucleotide (silent mutation) in the clone CDPK1 C3C.

Figure S9

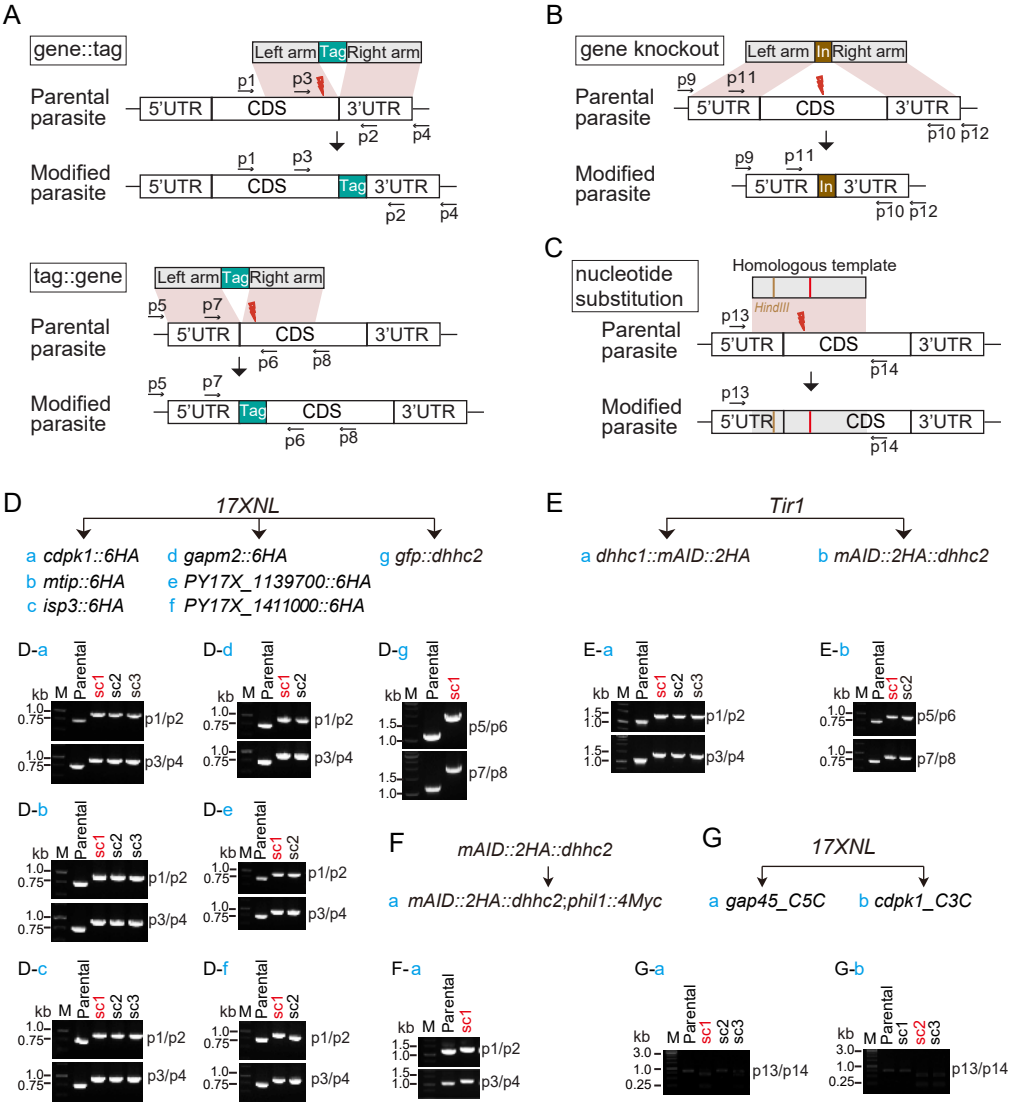
A
gene::tag
Left arm Tag Right arm
p1 p3
Parental parasite
5'UTR CDS 3'UTR
p2 p4
Modified parasite
5'UTR CDS Tag 3'UTR
tag::gene
p5 p7
p6 p8
B
gene knockout
Left arm In Right arm
p9 p11
p10 p12
C
nucleotide substitution
Homologous template
HindIII
p13
p14
D
17XNL
a cdpk1::6HA
b mtip::6HA
c isp3::6HA
d gapm2::6HA
e PY17X_1139700::6HA
f PY17X_1411000::6HA
g gfp::dhhc2
E
Tir1
a dhhc1::mAID::2HA
b mAID::2HA::dhhc2
F
mAID::2HA::dhhc2
a mAID::2HA::dhhc2;phil1::4Myc
G
17XNL
a gap45_C5C
b cdpk1_C3C
D-a
D-b
D-c
D-d
D-e
D-f
D-g
E-a
E-b
F-a
G-a
G-b
kb M Parental sc1 sc2 sc3
p1/p2
p3/p4
p5/p6
p7/p8
p13/p14

Supplementary Figure 9. Genotyping of genetically modified parasites in this study.
A-C. Schematic representation for CRISPR/Cas9 mediated gene modification, including the N-terminal and C-terminal tagging of genes with epitope tag (**A**), gene deletion (**B**), and nucleotide substitution (**C**) via double cross homologous recombination.
D-G. For each modification, both 5' and 3' homologous recombination was detected using gene specific PCR (Supplementary Table 2) to confirm successful integration of the homologous templates. Usually, one to three parasite clones (sc) for each modification were obtained after limiting dilution, and the clone indicated with red letter is used for further phenotype and functional analysis.